Topothermohaline convection – from synthetic simulations to reveal processes in a thick geothermal system

Attila Galsa[1,2], Márk Szijártó[1,3], Ádám Tóth[4], Judit Mádl-Szőnyi[3]

[1]Department of Geophysics and Space Science, Institute of Geography and Earth Sciences, ELTE Eötvös Loránd University, Budapest 1117, Hungary
[2]Institute of Earth Physics and Space Science, HUN-REN, Sopron 9400, Hungary
[3]József and Erzsébet Tóth Endowed Hydrogeology Chair, Department of Geology, Institute of Geography and Earth Sciences, ELTE Eötvös Loránd University, Budapest 1117, Hungary
[4]Copernicus Institute of Sustainable Development, Utrecht University, Utrecht 3584, The Netherlands

Correspondence to: Ádám Tóth (a.z.toth@uu.nl)

Abstract. Water table topography, temperature and solute content of groundwater all influence regional groundwater flow. Two-dimensional synthetic numerical calculations were performed to investigate the dynamic interaction between topography-driven forced convection and buoyancy-controlled free thermohaline convection. In the coupledcombined topothermohaline model, the recharge and flow-through zones are dominated primarily by topography-driven regional groundwater flow, which drifts warm upwellings towards the discharge zone. Beneath the discharge zone, a dome with high temperature, salinity and water age is formed, in which time-dependent thermohaline convection develops. It was established that (1) increasing the water table gradient suppresses the thermohaline dome, resulting in a near steady-state solution. (2) Increasing the bottom heat flux strengthens the warm upwellings, which ultimately leads to the break-up of the thermohaline dome, thus, paradoxically, reducing the average temperature. (3) Increasing the bottom salt concentration weakens the topography-driven groundwater flow, leading to the formation of a multilayered thermohaline dome with extremely high temperature, salinity and age. The operation of the topothermohaline model was demonstrated along a hydrogeological section crossing the Buda Thermal Karst (BTK), Hungary. We found that the unconfined karstic areas are dominated by topography-driven water flow, while in the confined, deep reservoirs, thermohaline convection is the prevailing flow regime. The thermally and compositionally mixed water promotes karstification and reaches the surface near the Danube River, the main discharge area. In the eastern, confined areas of BTK, significant amounts of heat may be retained on a geological time scale, making it a promising site for geothermal exploration.

1 Introduction

Deep and thick aquifers in sedimentary basins contain significant thermal water and mineral resources. Although limited knowledge of their physical flow processes exists, their exploitation is becoming increasingly needed worldwide. Fluid migration in basins is a key factor in the large-scale mobilization of heat and matter (Tóth, 1999; Ingebritsen et al., 2006; Bredehoeft 2018). Thus, revealing basins' flow and transport processes can help improve the success of exploiting targeted

resources (Czauner et al., 2022). These topics are especially significant because geothermal installations, new technologies for critical mineral production, and CO_2 sequestration use these aquifers for both fluid production and injection.

The eternal dilemma: What drives groundwater flow in sedimentary basins? The first mathematical answer was given by József Tóth, who revealed that ~~horizontal~~ variations in the water table can cause groundwater movement, especially in small (1–2 km deep) drainage basins. At least, he came to this conclusion through his simple, two-dimensional, homogeneous and isotropic analytical models (Tóth, 1962; 1963), which was later improved by Robinson and Love (2013), including stagnation point analysis and flow pattern asymmetry to reveal groundwater flow channels in a hierarchically nested system. The water table often follows the topography of the surface and can be considered as its~~a~~ subdued replica ~~thereof~~ — depending on climate, the slope of the surface, (hydro)geological conditions, etc (Haitjema and Mitchell-Bruker, 2005) —, resulting in the so-called topography-driven groundwater flow (Tóth, 2009; Bresciani et al., 2016), i.e. water table undulation controls the flow. Since the theory became widespread, several analytical studies have been carried out to make this simple but mathematically robust model more realistic (e.g. Freeze and Witherspoon, 1967), taking into account, for example, the rate of discharge vs depth dependence of permeability or permeability anisotropy (e.g. Jiang et al., 2009; 2011; Wang et al., 2011). The concept has achieved even greater success in numerical modelling, and has been able to explain the nature of groundwater flow in numerous cases (Winter and Pfannkuch, 1984; Gleeson and Manning, 2008), and its relationship with wetland distribution (Hayashi et al., 2016; Tóth et al., 2016; Simon et al., 2023), changes in groundwater-dependent ecosystems (Havril et al., 2018; Szabó et al., 2023; Fabiani et al. 2024), the complexity of groundwater flow system influenced by climate change (Trásy-Havril et al., 2022; Tsypin et al., 2024) the formation of dynamic hydrocarbon traps (Czauner and Mádl-Szőnyi, 2011; Wendebourg et al., 2018), the appearance of near-surface temperature anomalies, hot springs and flowing wells (An et al., 2015; Mádl-Szőnyi and Tóth, 2015; 2017; Jiang et al. 2020; Tóth et al., 2020; 2023). Topography-driven conceptual models are successful primarily in shallow depth ranges (Ferguson et al., 2023), where the role of other driving forces could generally be negligible.

As temperature increases, the density of water decreases (at least above 4 °C), and since in most geological environments, temperature increases with depth, thermal buoyancy develops in deeper parts of the groundwater basins. If the positive thermal buoyancy is sufficiently large, in other words, if the Rayleigh number of the system exceeds a critical value, free thermal convection occurs in both homogeneous and isotropic (Lapwood, 1948; Wooding, 1957; Elder, 1967) and inhomogeneous (Rubin, 1981) porous media. The onset and nature of convective flow is influenced by several factors, such as the Rayleigh number for the layer (Graham and Steen, 1994; Otero et al., 2004; Hewitt et al., 2014), the anisotropy of permeability (Smith and Chapman, 1983), the slope of the water table (Cserepes and Lenkey, 2004) etc. However, in terrestrial regions, the role of topography-driven water flow can rarely be ignored (Mádl-Szőnyi et al., 2023). One of these few cases is the phenomenon of deep confined geothermal reservoirs, e.g. in the Luttelgeest fractured carbonate platform, the Netherlands (Lipsey et al., 2016), in the fissured and karstic carbonate aquifer of Hainaut, Belgium (Licour, 2014), in the overpressured and fractured Mesozoic carbonate formation of Fábiánsebestyén, Hungary (Galsa et al., 2022a), etc.

65   Szijártó et al. (2019) performed a systematic simulation set in synthetic model domains to reveal the interaction between topography-driven forced and buoyancy-driven free thermal convection. They found that while the increasing layer thickness and temperature difference across the layer promote the dominance of free thermal convection, it is inhibited by the high gradient of the groundwater table and the permeability anisotropy. Since variations in the water table almost always influence groundwater flow in a real hydrogeological environment, most case studies — which do not neglect the effect of

70 temperature-dependence of water density — treat these two factors influencing groundwater flow together. Clauser and Villinger (1990) modelled the heat transport process in the sedimentary basin of Rheingraben, Germany, finding that free thermal convection intensifiesincreases heat transport, even if its presence is detectable only in certain parts of the model domain. 3D numerical model of heat transport in the Northeast German Basin suggests that topography-driven forced convection is the dominant heat transport process in shallow domains, while conduction is the dominant factor in deeper zones

75 (Kaiser et al., 2011; 2013a; Noack et al., 2013). However, they demonstrate that free thermal convection also affects heat transport locally. Lopez et al. (2016) explain the temperature and hydraulic head anomalies observed in the Lake Chad Basin by the phenomenon of mixed (i.e. combined forced and free) thermal convection developing in thick aquifers and being connected through faults. 3D but stationary model of the coupled topography-driven forced and buoyancy-driven free thermal convection is consistent with historical hydrogeological records and thermal anomalies observed in the Independence Basin,

80 Mexico (Ortega Guerrero, 2022).

   The solute content of groundwater varies over a wide range, from practically solute-free rainwater (<0.05 g l^{-1}) to sink-hole brines near the Dead Sea (519 g l^{-1}) (Weisbrod et al., 2016). Thus, total dissolved solids (TDS) also affect water density, with higher TDS resulting in higher water density, which creates a downward haline buoyancy. The problem of free haline convection and its analytical/numerical solution is very similar to the problem of free thermal convection (Weatherill et

85 al., 2004; Voss et al., 2010). Understanding the groundwater flow controlled by both topography and haline buoyancy is of high importance to coastal populations, as the increasing number and yield of producing wells facilitate subsurface seawater intrusion and salinization of freshwater aquifers (e.g. Barlow and Reichard, 2010; Hussain et al., 2019). In the interior of continents, the overproduction of water wells for agriculture, drinking water supply and energy use can lead to the mixing of different salinities and salinisation of soils (Yu et al., 2024). Numerical modelling of coupled topography-driven forced and

90 salinity-driven free convection revealed the complex flow regime beneath playas in the Great Basin, Utah, USA (Duffy and Al-Hassan, 1988), elucidated the variability of submarine groundwater discharge in a heterogeneous coastal volcanic aquifer near the Big Island of Hawaii, USA (Kreyns et al., 2020), characterized the mixed convection below a saline disposal basin depending on the haline Rayleigh number, the heterogeneity and anisotropy of the aquifer (Simmons and Narayan, 1997), determined the effect of saline water intrusion on the pattern of synthetic nested groundwater flow system (Zhang et al., 2020).

95 Galsa et al. (2022b) accomplished a sensitivity test to investigate the influence of salinity, permeability, anisotropy, heterogeneity, dispersivity and water table configuration on the groundwater flow and solute concentration. The operation of the mixed, so-called topohaline convection model was demonstrated in a realistic hydrogeological environment to explain the

connection between the upper siliciclastic and the deep karstic carbonate aquifers through the faulted clayey aquitard with high TDS.

100   In thermohaline convection, the free positive thermal and negative haline convection play a competitive role, when both the temperature and the salinity increase with depth. The onset of thermohaline convection was determined analytically in simple homogeneous Boussinesq models for different boundary conditions by Nield (1968), and in heterogeneous (layered) aquifers by Rubin (1982a; 1982b). Szijártó and Galsa (2020) studied the stationary and time-dependent character of thermohaline convection in their two-dimensional synthetic numerical models. In real hydrogeological situations, however,
105 the effect of forced convection induced by the groundwater table configuration cannot be neglected. Thus, de Hoyos et al. (2012) investigated the 'thermohaline' effects on 3D groundwater flow forming in the Paris sedimentary Basin, France, but they concluded that the influence of the pressure and temperature on the water density is insignificant (<3%), so the role of thermal buoyancy was ignored. Gupta et al. (2015) applied a fully coupled topothermohaline numerical model to determine the age and origin of brines in the Alberta Basin, Canada. Based on transient simulations, regional, topography-driven
110 groundwater flow characterizes the shallow formations in the Tiberias Basin, while deep-seated thermohaline convection cells develop in thick, covered carbonate sequences (Magri et al., 2015).

        The Buda Thermal Karst (BTK), Hungary, is an area with high geothermal potential, but also a complex groundwater flow and thermal regime owing to the fact that the karstified carbonates are mostly unconfined on the western side and confined on the eastern side (Mádl-Szőnyi and Tóth, 2017). Therefore, Szijártó et al. (2021) carried out an extensive numerical study to
115 clarify the role of different heat transport processes, separating the phenomena of conduction, forced and free thermal convection. Simulations showed that different heat transport processes dominate in distinct regions of the karst system, while free thermal convection, developed mainly in deeper and confined reservoirs, formed in all model calculations. Havril et al. (2016) studied the flow and heat transport processes in the karstified reservoir from the perspective of the geological evolution of BTK. Based on their numerical model results, it can be stated that with the uplift and erosion of the cover on the western
120 side, the topography-induced forced convection has been enhanced at the expense of free thermal convection, but the latter is still operating in the present system, mainly in the deeper, covered carbonates. Although most recent karst waters are freshwater (rarely brackish), they were filled up by marine water, when the system was confined~~formed in a marine environment~~. Additionally, the clayey cover layer on the eastern side still contains saline water, which is presumably connected to the water flows in the confined karst (Mádl-Szőnyi et al., 2019). In such a hydrogeological setting, both topography-driven forced
125 convection and free thermohaline convection can influence the coupled flow-thermal-saline regime, forming an interconnected geothermal reservoir.

        In all real cases, the terrestrial groundwater flow system is controlled by the dynamic interaction of topography-driven forced convection and density-driven free thermal and haline convection. Still, in most models, the numerical modeller switches off one or two components of driving forces to reduce computational demands. Sometimes, this is not a problem,
130 especially if one component of the system is significantly under-dominated, and consequently, the model can produce solutions that are close to reality. However, in deep basins, where distinct geological formations have different hydraulic, thermal and

salinity properties, it inevitably leads to oversimplification of the groundwater flow system. Moreover, in such complex, non-linear systems, small interventions in the model parameters can lead to radically different solutions.

Therefore, the main goal of this paper is to (1) present an extensive parameter analysis in a two-dimensional synthetic

135 model domain emphasizing the complex character of the groundwater flow as a dynamic equilibriumbalance between the topography-driven forced and buoyancy-driven free thermohaline convection. The flow, the temperature and the salinity of the topothermohaline system are stimulated directly by the water table configuration, the heat flux and salt concentration prescribed along the bottom of the model domain, respectively. However, the other two variables are also affected in the fully coupled system. Control parameters, such as the average Darcy flux, the solute concentration, the temperature, and the water

140 age are computed for both the whole model basin and the different salinity zones to characterize the flow systems quantitatively. Second, (2) the operation of the topothermohaline convection model is demonstrated in a thick carbonate system, the Buda Thermal Karst (BTK) system, which has a high geothermal potential (Mádlné Szőnyi et al., 2018; Mádl-Szőnyi et al., 2019; Mádl-Szőnyi, 2019; Kun et al., 2024). This study is the first to systematically investigate the phenomenon of topothermohaline convection through synthetic numerical modelling and the first attempt to explore the coupled

145 groundwater flow, thermal and salinity character of BTK, Hungary.

2 Model description

2.1 Physical background

The topothermohaline problem is treated numerically by solving the coupled continuity equation (1), Darcy's law (2), and the heat (3) and mass (4) transport equations (Nield and Bejan, 2017), which govern the conservation of mass and momentum,

150 and the transport of heat and solute concentration in subsurface water flow, respectively,

$$\Phi \frac{\partial \rho_w}{\partial t} + \nabla(\rho_w \mathbf{q}) = 0, \tag{1}$$

$$\mathbf{q} = -\frac{\mathbf{k}}{\mu}(\nabla p + \rho_w g \nabla z), \tag{2}$$

$$\left[\Phi \rho_w c_{pw} + (1 - \Phi)\rho_m c_{pm}\right]\frac{\partial T}{\partial t} = -\rho_w c_{pw} \mathbf{q} \nabla T + \nabla\{[\Phi \lambda_w + (1 - \Phi)\lambda_m]\nabla T\}, \tag{3}$$

$$\Phi \frac{\partial c}{\partial t} = -\mathbf{q}\nabla c + \nabla[(\Phi D_{diff}\mathbf{I} + \mathbf{D_{disp}})\nabla c], \tag{4}$$

155 where $\mathbf{q}$, p, T and c are the unknown Darcy flux, pressure, temperature and solute concentration, Φ, $\mathbf{k}$, μ, g, D_{diff} and $\mathbf{D_{disp}}$, t, z and $\mathbf{I}$ denote the porosity, the diagonal permeability tensor, the dynamic viscosity of water, the gravitational acceleration, the molecular diffusion of water, the mechanical dispersion tensor, the time, the vertical coordinate and the identity matrix, respectively. ρ, c_p and λ are the density, the specific heat and the thermal conductivity of the water and the matrix denoted by subscripts w and m, respectively. The dispersion tensor is determined by the longitudinal and transverse dispersivity (α_L and

160 α_T), where the value of α_T was fixed as $\alpha_T = \alpha_L/10$. In the synthetic models, dispersivity was assumed to be zero, and the

permeability was isotropic, while in the real hydrogeological simulation, α_L=100 m and anisotropic permeability ($\varepsilon=k_x/k_z>1$) were applied. Constant model parameters for the synthetic model are given in Table 1.

The numerical modelling of topothermohaline convection had to take into account the dependence of water density, $\rho_w(T,p,c)$, on temperature (sixth-order polynomial) and pressure (second-order polynomial) (Magri, 2009), as well as on concentration (linear) (Kohfahl et al., 2015). Molecular diffusion, $D_{diff}(T)$, is strongly dependent on temperature, which was considered in the simulations using a quadratic Arrhenius law (Easteal et al., 1989). Quantitative relationships of the temperature-, pressure- and concentration-dependence of water density and molecular diffusion are reported in the Supplementary material. In order to calculate the age of the groundwater, the mean age was computed by solving the age mass equation defined by Goode (1996). Goode (1996) proposedsupposed that water age propagates through the porous medium in the same way as solute, by advection, diffusion and dispersion,

$$\Phi\frac{\partial \tau}{\partial t} = -\mathbf{q}\nabla\tau + \nabla\left[\left(\Phi D_{diff}\mathbf{I} + \mathbf{D_{disp}}\right)\nabla\tau\right] + \Phi, \tag{5}$$

where τ denotes the mean age of the groundwater, and the last additive term in Eq. (5) represents that the water age increases with time. Thus, Eq. (5) was solved by coupling to Eq. (1)–(4), where water age is influenced by the Darcy flux through the terms of advection and dispersion, and by the temperature through molecular diffusion, $D_{diff}(T)$. Certainly, water age has no effect on thermohaline convection.

Table 1. Parameters of the synthetic model

Description	Symbol	Value	Unit
Porosity	Φ	0.1	1
Permeability	k	10^{-13}	m^2
Gravitational acceleration	g	9.81	$m\ s^{-2}$
Reference water density	ρ_{ref}	999.79	$kg\ m^{-3}$
Dynamic viscosity of the water	μ	$5\cdot10^{-4}$	Pa s
Matrix density	ρ_m	2450	$kg\ m^{-3}$
Specific heat of water	c_{pw}	4200	$J\ kg^{-1}\ K^{-1}$
Specific heat of matrix	c_{pm}	900	$J\ kg^{-1}\ K^{-1}$
Thermal conductivity of water	λ_w	0.6	$W\ m^{-1}\ K^{-1}$
Thermal conductivity of matrix	λ_m	2	$W\ m^{-1}\ K^{-1}$
Longitudinal dispersivity	α_L	0	m
Transverse dispersivity	α_T	0	m

2.2 Numerical model

Synthetic model simulations were carried out in a two-dimensional, simple, homogenous, isotropic model domain without
180   dispersion to concentrate on the hydrogeophysical behaviour of the system. The length and the average depth of the model domain are L=40 km and d=5 km, respectively (Fig. 1). Boundary conditions for the flow are no-flow along the side walls and the bottom, the regional groundwater flow is driven by a cosinusoidal water table (e.g. Domenico and Palciauskas, 1973; Wang et al., 2015; Zhang et al., 2018) with an amplitude of H=50 m in the base model,

$$z_{wt}(x) = -H \cos\left(\frac{\pi x}{L}\right), \tag{6}$$

185   where x denotes the horizontal coordinate. The water table, z_{wt}, corresponds to the top of the model domain, resulting in a topography-driven groundwater flow from right to left (Fig. 1.a). Constant temperature and constant heat flux boundary conditions for the heat transport were applied along the upper and lower boundaries, respectively, while vertical boundaries were considered thermally insulating. Salt concentration along the horizontal boundaries was fixed, with a value of zero on the surface due to precipitation infiltration. Fixed value along the bottom allows diffusive and/or dispersive salinity influx from deeper impervious formations. Concentration flux was not allowed through the side walls. The surface boundary condition for
190   the water age is an open boundary representing that the age of recharging water is zero, and the 'age mass' discharges from the model with the water,

$$\tau_s = \begin{cases} 0 & if \ \mathbf{nq} < 0 \quad (recharge) \\ \mathbf{n}D_{diff}\nabla\tau = 0 & if \ \mathbf{nq} > 0 \quad (discharge) \end{cases}, \tag{7}$$

where $\mathbf{n}$ is the normal vector of the surface. Other boundaries were closed similarly to flow conditions are summarized in
195   (Fig. 1).
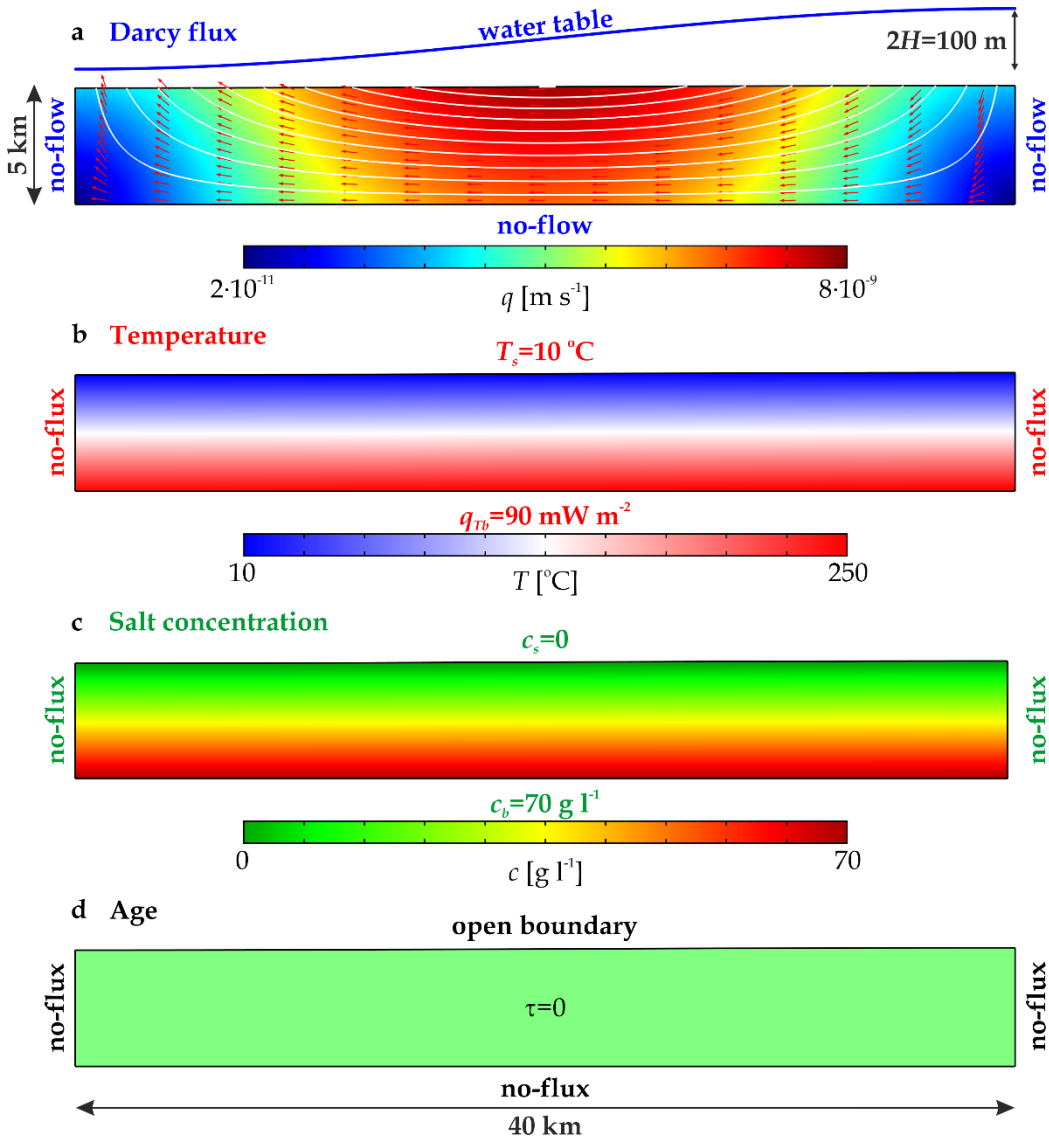
Figure 1. Initial and boundary conditions in the synthetic base model for (a) the flow, (b) the temperature, (c) the salt concentration and (d) the groundwater age. (a) White streamlines and red arrows illustrate the direction of topography-driven groundwater flow.

200   The initial condition for the Darcy flux is obtained from the solution of Eqs (1)–(2) using reference water density. Initial conditions for the temperature and the salt concentration come from conductive and diffusive solutions of heat (Eq. (3)) and mass (Eq. (4)) transport equations, respectively. Initially, the water age was zero over the entire model domain (Fig. 1).

The topothermohaline convection model was solved numerically using COMSOL Multiphysics 5.3a, a finite element software package (Zimmerman, 2006). The synthetic model domain was discretized by approx. 57 000 triangular finite

205   elements depending on the groundwater table amplitude, H. The mMaximum size of finite elements was 100 m, but boundary elements with a thickness of 100 m/8 were applied along the boundaries to consider high gradients of the variables. Pressure

and Darcy flux were approximated by quadratic functions, while temperature, concentration and age were assumed to be linear within the finite elements. Time stepping was increased exponentially to 1000 yr, then it was linear with a maximum time step of 100 yr. Calculations were carried out to reach the quasi-stationary solution, which required 2–10 Myr depending on H. In general, higher water table amplitude stabilized the system and resulted in a faster quasi-stationary solution. Using this parameter setup, one simulation consumed approx. 5 GB memory and 30–540 hours CPU time on an Intel Server with 2 Xeon Gold processors. Overall, 29 time-dependent synthetic numerical simulations were performed to reveal the character of topothermohaline convection in basin-scale groundwater flow. The numerical model built in COMSOL Multiphysics has been tested in many hydrogeological situations (for heat/solute/age transport calculations) and has been quantitatively verified (e.g. Szijártó et al., 2019; Galsa et al., 2022b; Szijártó et al., 2054).

2.2 Model parameterization

In the synthetic simulation set, three parameters, the water table amplitude, H, the bottom heat flux, q_{Tb} and the bottom salt concentration, c_b, were varied systematically to investigate their direct influence on the Darcy flux, the temperature and the salinity, respectively. Clearly, in a coupled system, e.g. increasing H not only affects the flow but also indirectly influences the other parameters. ~~The parameters of the base model and the parameter intervals applied in synthetic simulations are summarized in Table 2.~~ The parameter ranges were chosen to include the most common examples of groundwater basins regarding both water table amplitude (e.g. Conlon et al. 2005; Wang et al., 2015), bottom heat flux (e.g. Pollack and Chapman, 1977; Pollack et al., 1993; Kolawole and Evenick, 2023) and bottom salt concentration (e.g. Birkle et al., 2009; Bagheri et al., 2014; Kohfahl et al., 2015; Jiang et al., 2024), as well as the case of the Buda Thermal Karst. The parameters of the base model applied in synthetic simulations are considered as an average value and are summarized in Table 2, together with the parameter ranges.

The effects of model parameters were investigated and will be presented in three different ways:

- Snapshots of the calculated Darcy flux, temperature, salt concentration, salinity zone and age distribution after the system reached the steady-state solution illustrate the behaviour of topothermohaline convection.
- The spatially and temporally averaged control parameters, such as mean Darcy flux (q_{av}), temperature (T_{av}), concentration (c_{av}) and water age (τ_{av}), quantify the role of the model parameters on the complex flow system. The spatial averaging is not only performed for the full model domain but also for the four salinity zones defined by Deming (2002) for freshwater (0–1 g l^{-1}), brackish water (1–10 g l^{-1}), saline water (10–100 g l^{-1}) and brine water (>100 g l^{-1}) zones. The relative area of each salinity zone (A) is also shown.
- Animations of the variables in the Supplementary material (Galsa et al., 2025) facilitate understanding the dynamics of topothermohaline convection in synthetic groundwater basins.

Table 2. Model parameters of the base model and the studied parameter range.

Description	Symbol	Base model	Interval	Unit
Water table amplitude	H	50	5–500	m
Bottom heat flux	q_{Tb}	90	50–120	mW m^{-2}
Bottom salt concentration	c_b	70	2–200	g l^{-1}

3 Results

3.1 Synthetic simulations

In this chapter, we present the behaviour of the flow/thermal/solute/age mass system in the synthetic base model. Then, the effect of the groundwater table amplitude, the heat flux and salt concentration prescribed at the bottom of the model domain on the control parameters will be systematically investigated.

3.1.1 Base model

In the base model, the constant model parameters listed in Table 1 characterize the basin, while the water table amplitude, the bottom heat flux and salt concentration were fixed at H=50 m, q_{Tb}=90 mW m^{-2} and c_b=70 g l^{-1} (Table 2), respectively. Fig. 2 shows the quasi-stationary solution of the Darcy flux, the temperature, the salt concentration and the salinity zones, as well as the water age at t=3 Myr after the initial state. Three main zones are separated: (1) the middle part of the basin is dominated by topography-driven regional groundwater flow. This domain is characterized by cool (T<20 °C), fresh (c<1 g l^{-1}) and young (τ<10 kyr) water. Hot and saline plumes are forming at the bottom of the model, and drifting to the left, towards the discharge zone driven by the topography-driven groundwater flow (Fig. 2.b and c). On the other hand, (2) a quasi-stationary thermohaline dome is forming beneath the discharge zone, in which hot (T>100 °C), saline (c>40 g l^{-1}) and aged (τ>400 kyr) water is convecting. At the margin of the two zones, plumes driven by the regional groundwater flow are climbing up the thermohaline dome, resulting in a maximum of Darcy flux (Fig. 2.a). Intense flow is noticed inside the dome, where thermohaline convection is vigorous. (3) The weak thermohaline convection zone beneath the recharge area (right) is the combined consequence of the cold downward flow, the upward thermal buoyancy and the no-flow vertical boundary condition (Szijártó et al 2019). Animation S1 in the Supplementary material (Galsa et al., 2025) illustrates the dynamic balance between the topography-driven forced and thermohaline buoyancy-driven free convection in the base model.

a Darcy flux

5 km

0   q [m s^{-1}] $2 \cdot 10^{-8}$

b Temperature

10   T [$^{\circ}$C]   137

c Concentration

0   c [g l^{-1}]   70

d Salinity

fresh   brackish   saline

e Age

40 km

0   τ [kyr]   600
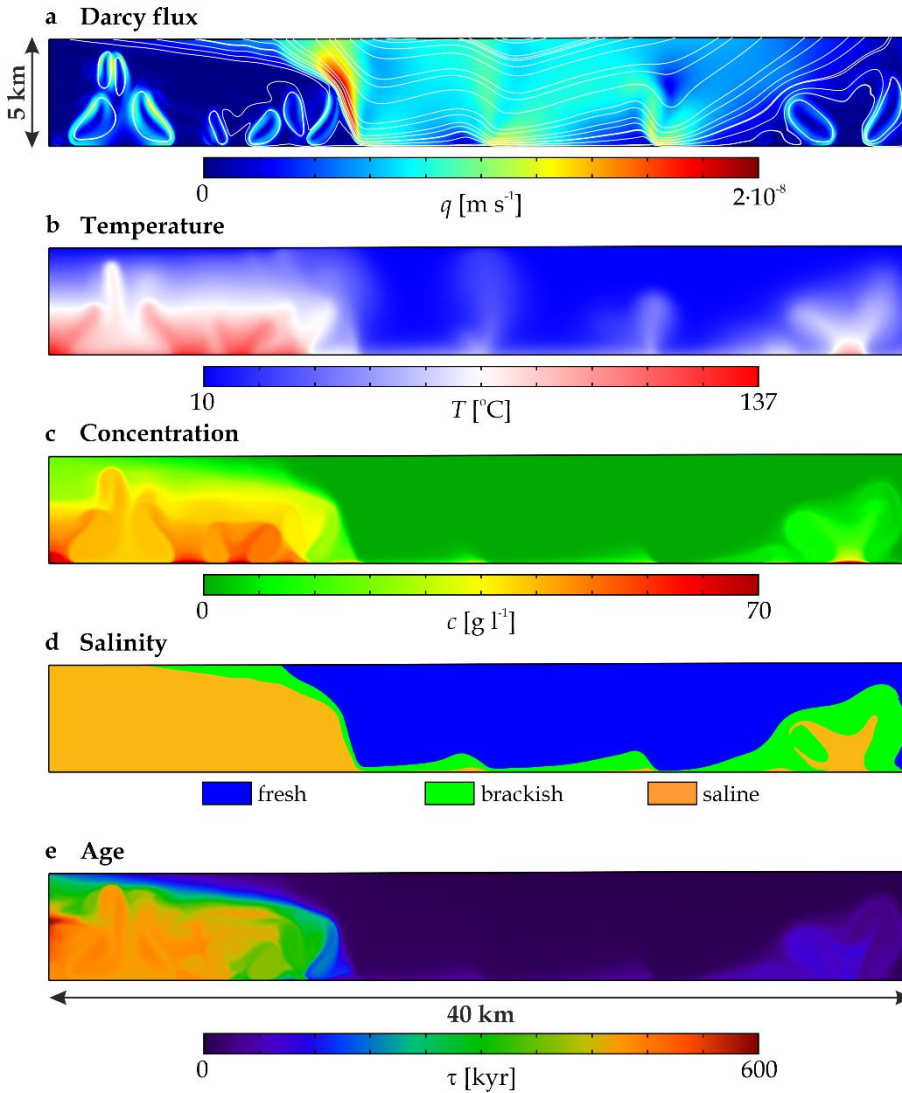
Figure 2. Snapshots of the (a) Darcy flux, (b) temperature, (c) salt concentration, (d) salinity zones and (e) water age at t=3 Myr after the initial state in the base model (Table 1 and 2). (a) Streamlines illustrate the flow direction. (d) Salinity zones: freshwater (blue), brackish water (green) and saline water (orange).

3.1.2 Effect of water table amplitude

In this part, only the water table amplitude was varied in the range of H=5 m and 500 m (e.g. Conlon et al. 2005; Wang et al., 2015), and other model parameters (q_{Tb}, c_b) were kept fixed according to the base model (Table 2). The water table amplitude, in other words, the magnitude of the hydraulic gradient, directly influences the intensity of the topography-driven groundwater flow. Figure 3 presents two model calculations having low, H=20 m (left) and high, H=200 m (right) water table amplitudes. At low hydraulic gradients (H=20 m), regional water flow is weak to suppress thermohaline convection. Thus, a major part of the basin is saturated by saline, warm and aged water (Fig. 3.b–e, left panel). The topography-driven flow is only detected in

a thin band, in the upper right part of the model domain. Intense free convection occurs in the thermohaline layer (Animation S2 in Galsa et al., 2025). In the absence of a significant regional groundwater flow, the solution is time-dependent and converges only slowly to the quasi-stationary solution. In contrast, at high water table amplitude (H=200 m), regional flow dominates the system with a Darcy flux distribution analogous to the solution with constant water density (Fig. 3.a cf. Fig. 1.a). Strong topography-driven forced convection flushes heat and solutes out of the basin, resulting in cold, fresh, young water over a large part of the model domain (Fig. 3.b–e, right panel). The thermohaline dome shrinks in the deeper part of the discharge zone, leading to a weakly time-dependent numerical solution (Animation S3 in Galsa et al., 2025).
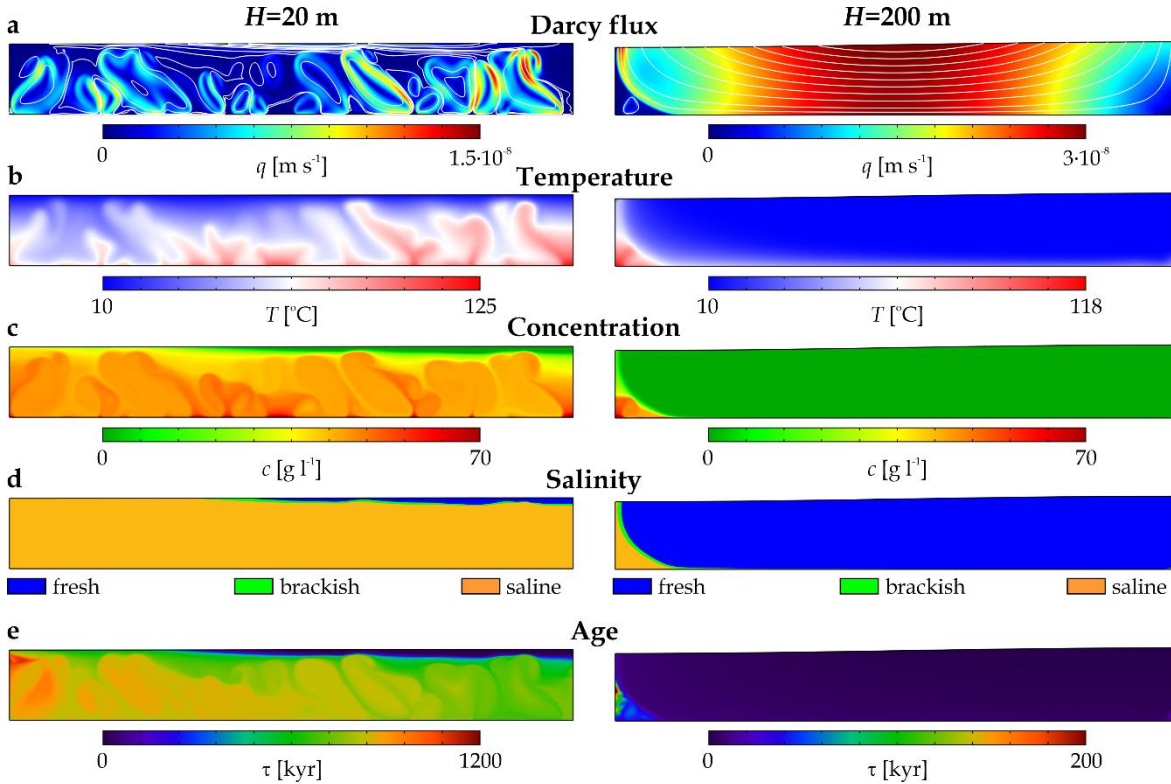
Figure 3. Numerical solutions of (a) the Darcy flux, (b) the temperature, (c) the salt concentration, (d) the salinity zones and (e) the water age at water table amplitudes of H=20 m (left panel) and H=200 m (right panel). The quasi-stationary solutions are shown at 10 Myr (left) and 2 Myr (right).

Figure 4 quantifies the effect of the water table amplitude on the relative area, Darcy flux, temperature, concentration and water age of the salinity zones and the total model domain. Figure 4.a proves that at low water amplitude ($H \leq 20$ m), the saline zone controls more than 90% of the basin due to the dominance of thermohaline convection. On the other hand, at high water table amplitude ($H \geq 200$ m), the freshwater zone prevails over the majority of the basin (>90%) due to the intense topography-driven forced convection. Between the two extremes, the role of topography-driven groundwater flow becomes more intense as H increases. The thermohaline layer that fills most of the basin becomes a dome and shrinks to the deeper

regions of the discharge zone. Higher values of standard deviation indicate that this transition interval (H=20–200 m) is
strongly time-dependent. In the region dominated by thermohaline convection ($H \leq 20$ m), the average Darcy flux is equal to
that in the saline zone, $q_{av} \approx 3 \cdot 10^{-9}$ m s^{-1}. While the appearance of the freshwater zone intensifies the flow, the average Darcy
flux increases approx. linearly following the Darcy's Law (Eq. (2)) (Fig. 4.b). In the thermohaline convection-dominated
domain, the average temperature (46–57 °C), salt concentration (45–41 g l^{-1}) and water age (981–726 kyr) of the basin are
characterised by the saline zone (Fig. 4.c–e). However, forced convection driven by the increasing water table amplitude
effectively sweeps heat, salt and aged water out of the basin, resulting in an intense flow of cold, fresh and young groundwater.
It is worth noting that (1) water age and salt concentration are very sensitive to the presence of topography-driven groundwater
flow, decreasing by almost three and two orders of magnitude, respectively, with increasing H. (2) The temperature,
concentration and age of the saline zone exceed the values of the freshwater zone in all simulations.
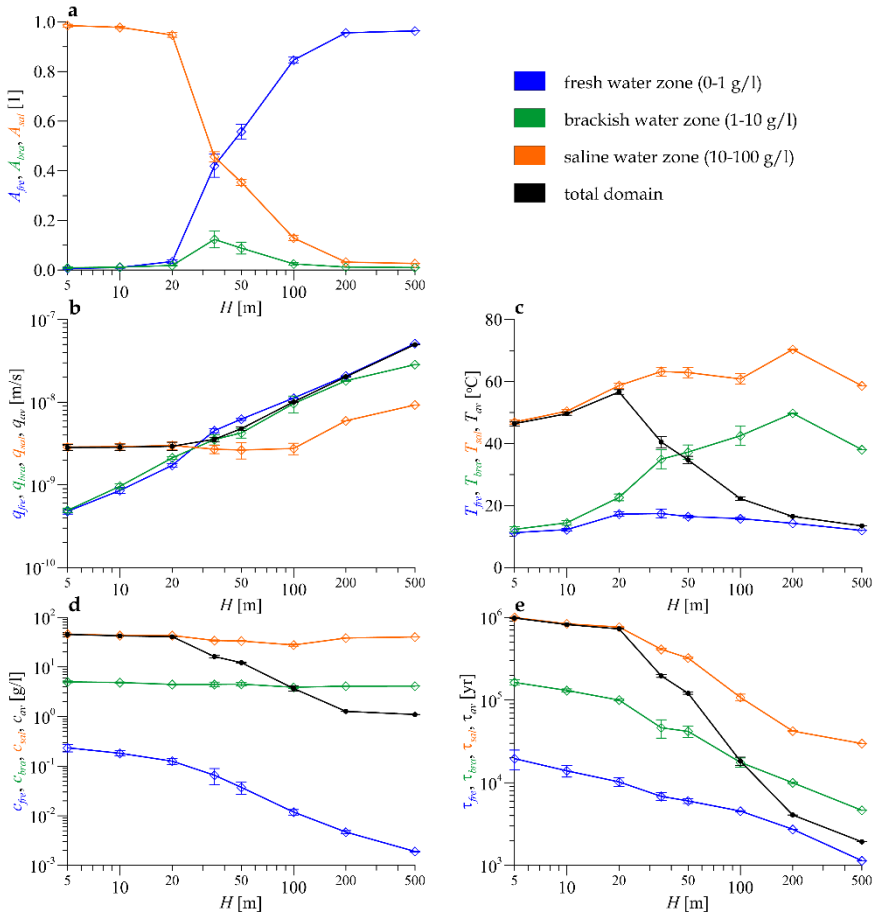
Figure 4. (a) The relative area, (b) the Darcy flux, (c) the temperature, (d) the concentration and (e) the age of the salinity zones plotted against the water table amplitude. Each salinity zone is marked with a different colour. The values averaged for the whole model domain are shown in black. Standard deviations calculated for the quasi-stationary phase of the time series are marked by error bars.

3.1.3 Effect of bottom heat flux

The heat flux in the continental crust varies over a wide range (e.g. Pollack and Chapman, 1977; Pollack et al., 1993; Kolawole and Evenick, 2023), which directly influences the temperature distribution and, thus the character of topothermohaline convection. At low bottom heat flux, q_{Tb}=50 mW m^{-2} (Fig. 5, left panel), the quasi-stationary solution is similar to the base model (Fig. 2). The model domain in the middle part and below the recharge zone is dominated by topography-driven groundwater flow. While beneath the discharge zone, a thermohaline dome is formed where warm, saline and aged water is convecting (Animation S4 in Galsa et al., 2025). The temperature of the dome is lower than in the base model due to the lower heat flux. Therefore, the thermohaline convection is more sluggish ($q_{sal}\approx 1.5 \cdot 10^{-9}$ m s^{-1}), smaller in extent, and contains older water compared to the base model. On the other hand, the high bottom heat flux increases the role of thermal buoyancy and results in strong free thermal convection (Fig. 5, right panel). The warm upwellings evolving at the bottom of the basin drift with the regional water flow towards the discharge zone, resulting in Darcy flux, concentration and age perturbations in the topography-dominated zone. Animation S5 (Galsa et al., 2025) qualitatively suggests that the thermal buoyancy is so strong that it overcomes the negative haline buoyancy and significantly weakens the thermohaline dome beneath the discharge zone.
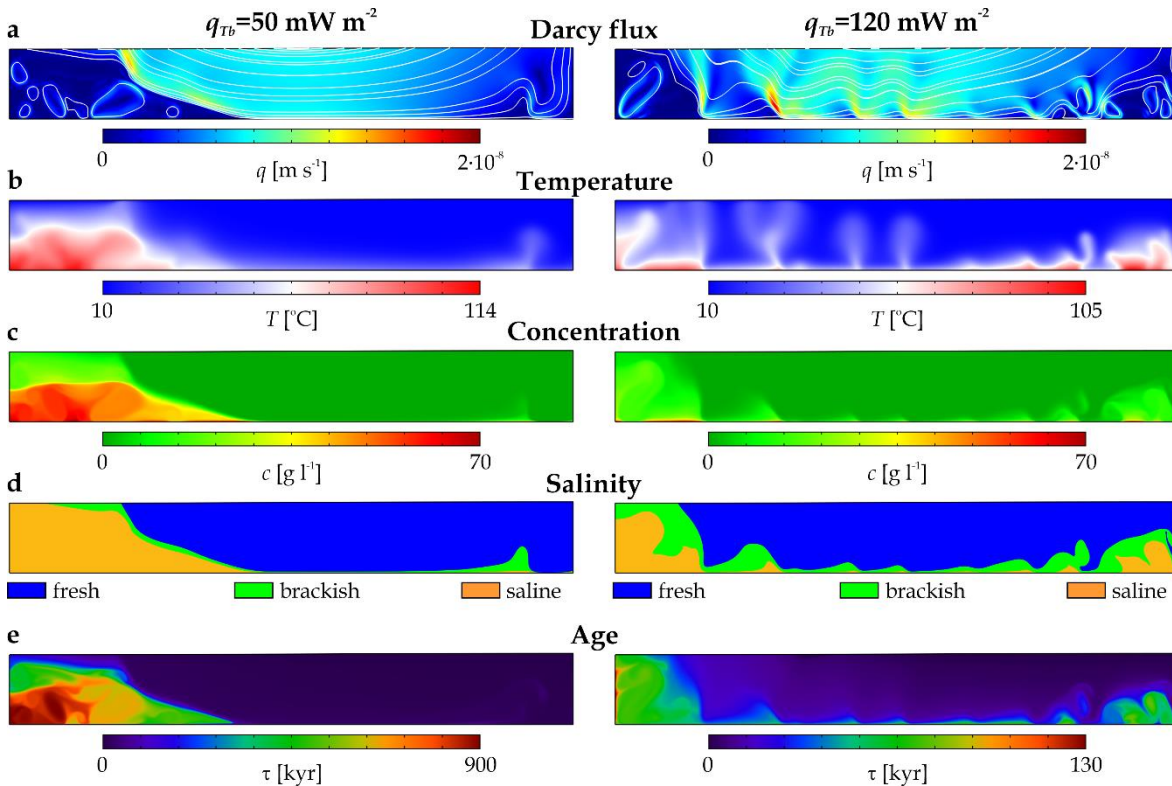
Figure 5. Numerical solutions of (a) the Darcy flux, (b) the temperature, (c) the salt concentration, (d) the salinity zones and (e) the water age at bottom heat fluxes of q_{Tb}=50 mW m^{-2} (left panel) and q_{Tb}=120 mW m^{-2} (right panel). The quasi-stationary solutions are shown at 3 Myr (left) and 2 Myr (right).
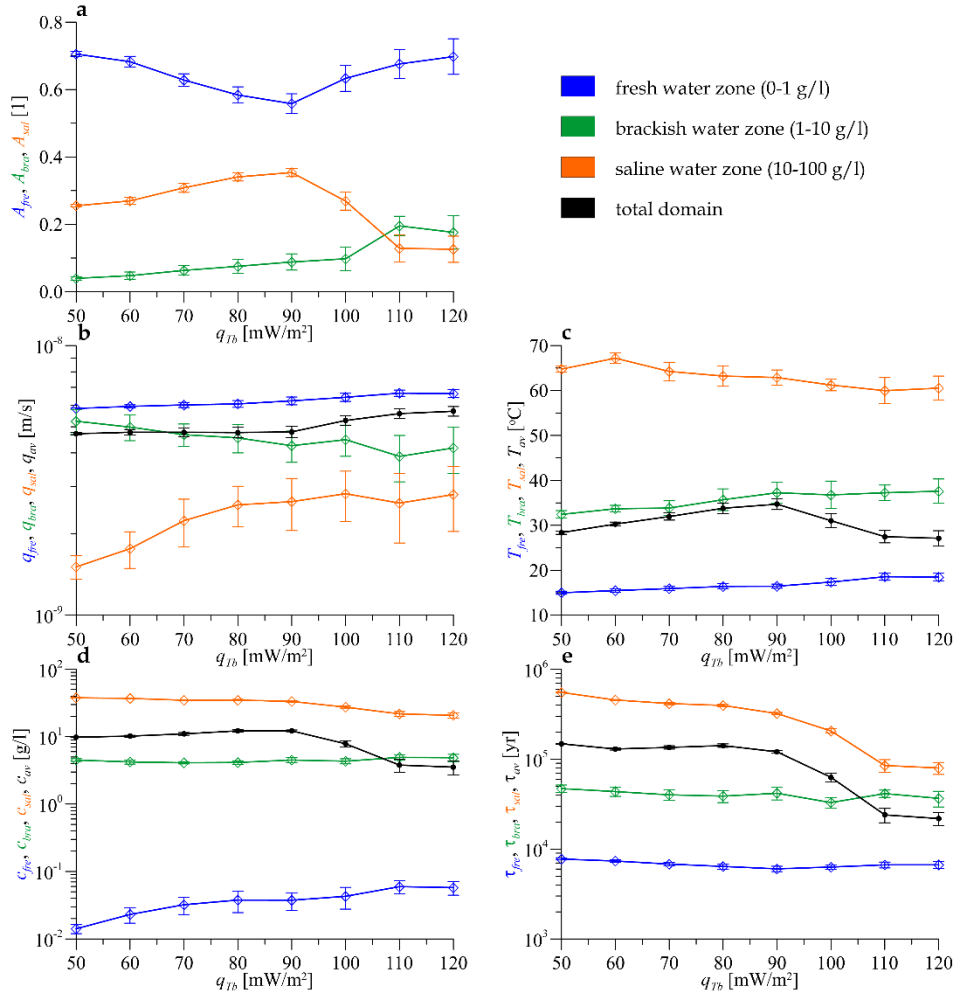
Figure 6. (a) The relative area, (b) the Darcy flux, (c) the temperature, (d) the concentration and (e) the age of the salinity zones
325 **plotted against the bottom heat flux. Each salinity zone is marked with a different colour. The values averaged for the whole model**
domain are shown in black. Standard deviations calculated for the quasi-stationary phase of the time series are marked by error
bars.

The variation of the control parameters supports the conclusions drawn from the qualitative solutions, that is, the dual

role of the bottom heat flux. Increasing the bottom heat flux in the range of q_{Tb}=50–90 mW m^{-2} facilitates the development of

330 the thermohaline dome, increasing its size and thus the average temperature of the model (Fig. 6.a and c), as well as the

intensity of convection within the salt dome (Fig. 6.b). However, for higher heat fluxes (q_{Tb}>90 mW m^{-2}), the behaviour of the

topothermohaline system changes. Intense thermal convection breaks down the thermohaline dome, increasing the relative

area of the freshwater and brackish zone (Fig. 6.a). For the whole basin, this results in a faster flow, lower average temperature,

lower salinity and younger waters (Fig. 6.b–e). Even though the cause is quite different, the behaviour of the control parameters

335 is similar to the influence of the increasing water table amplitude. It is, therefore, important to emphasise that a higher bottom

heat flux can — paradoxically — also lead to lower temperatures, as vigorous thermal convection also drives heat itself out of the basin by breaking up the hot thermohaline dome beneath the discharge zone.

3.1.4 Effect of bottom solute concentration

Groundwater basins are often located above a low-permeability basement, whose salinity can vary strongly depending, for example, on the presence of evaporites, pore water salinity, etc (e.g. Birkle et al., 2009; Bagheri et al., 2014; Kohfahl et al., 2015; Jiang et al., 2024). Figure 7 shows two snapshots of quasi-stationary numerical solutions with prescribed solute concentration at the bottom boundary of the basin of c_b=10 g l^{-1} (left panel) and c_b=200 g l^{-1} (right panel). Other parameters agree with the values of the base model (Table 2). At low salinities, topography-driven forced convection and free thermal convection together control the flow regime. As a consequence, the negative haline buoyancy is negligible, and no thermohaline dome is formed. Topography-driven regional flow is perturbed by warm plumes rising from the bottom of the basin and drifting towards the discharge zone (Animation S6 in Galsa et al., 2025). The majority of the basin is saturated by cold, young freshwater, and the thermal plumes ascend to the surface unopposed, resulting in lower temperatures. The quasi-stationary plume of warm, brackish and aged water on the right side of the model domain is the result of the dynamic equilibrium of infiltrating cold water, rising warm water and a no-flow side boundary. In the model where high salinity is prescribed at the bottom of the basin (Fig. 7, right panel), the negative haline buoyancy is sufficiently large for the formation of a thermohaline dome. The high density of salt water effectively retains heat and discharge flux, resulting in extremely high temperatures and water ages, even in the homogeneous basin, respectively. Spontaneous stratification develops inside the dome, with three layers characterized by separate thermohaline convection (Animation S7 in Galsa et al., 2025). In the multilayer thermohaline dome, the salt concentration and the age of the layers increase with depth.

355
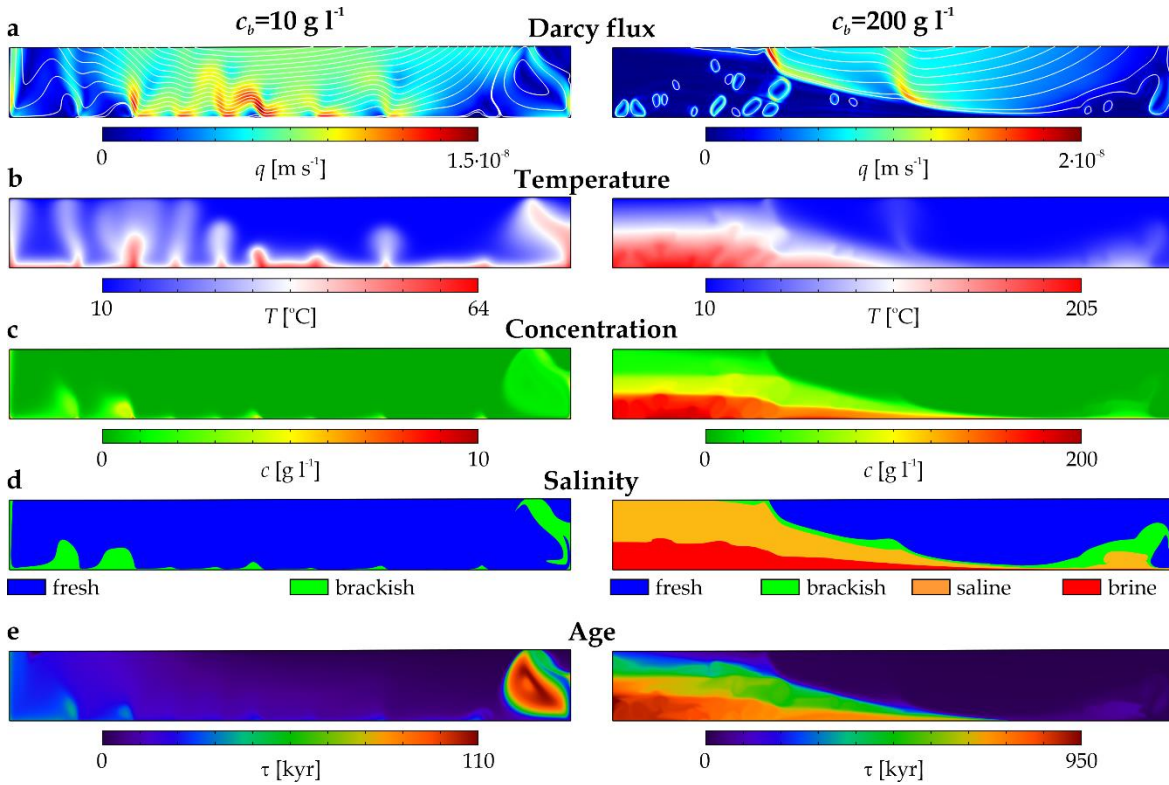
Figure 7. Numerical solutions of (a) the Darcy flux, (b) the temperature, (c) the salt concentration, (d) the salinity zones and (e) the water age at the bottom salt concentration of c_b=10 g l^{-1} (left panel) and c_b=200 g l^{-1} (right panel). The quasi-stationary solutions are shown at 2 Myr.

360   The control parameters indicate that as c_b increases, the freshwater zone shrinks, although the reduction of the relative area (A_{fre}) stops at $c_b \geq 100$ g l^{-1}, and its extent does not fall below 40% even at extremely high salinity (Fig. 8.a). While c_b increases by 2 orders of magnitude (from 2 to 200 g l^{-1}), the average salinity of the basin increases by more than 3 orders of magnitude from c_{av}=0.031 to 37.2 g l^{-1} (Fig. 8.d). The explanation is that the high salinity slows down the flow (Fig. 8.b) and reduces the advective mass transport, which thus acts as a positive feedback. The mass transport is accompanied by a reduction

365   in heat transport, which increases the average temperature of the basin by about 30 °C from T_{av}=21.6 to 53.4 °C, clearly caused by the appearance of saline and brine waters (Fig. 8.c). As the concentration of the lower boundary increases, the average water age of the basin increases by more than one order of magnitude (from τ_{av}=14.4 to 218 kyr), also due to the increasing dominance of saline/brine and aged waters (Fig. 8.e). It is maintained that moving from the freshwater zone to the brine water zone slows down the flow, while the temperature, solute concentration (it is trivial) and age of the water gradually increase.

370
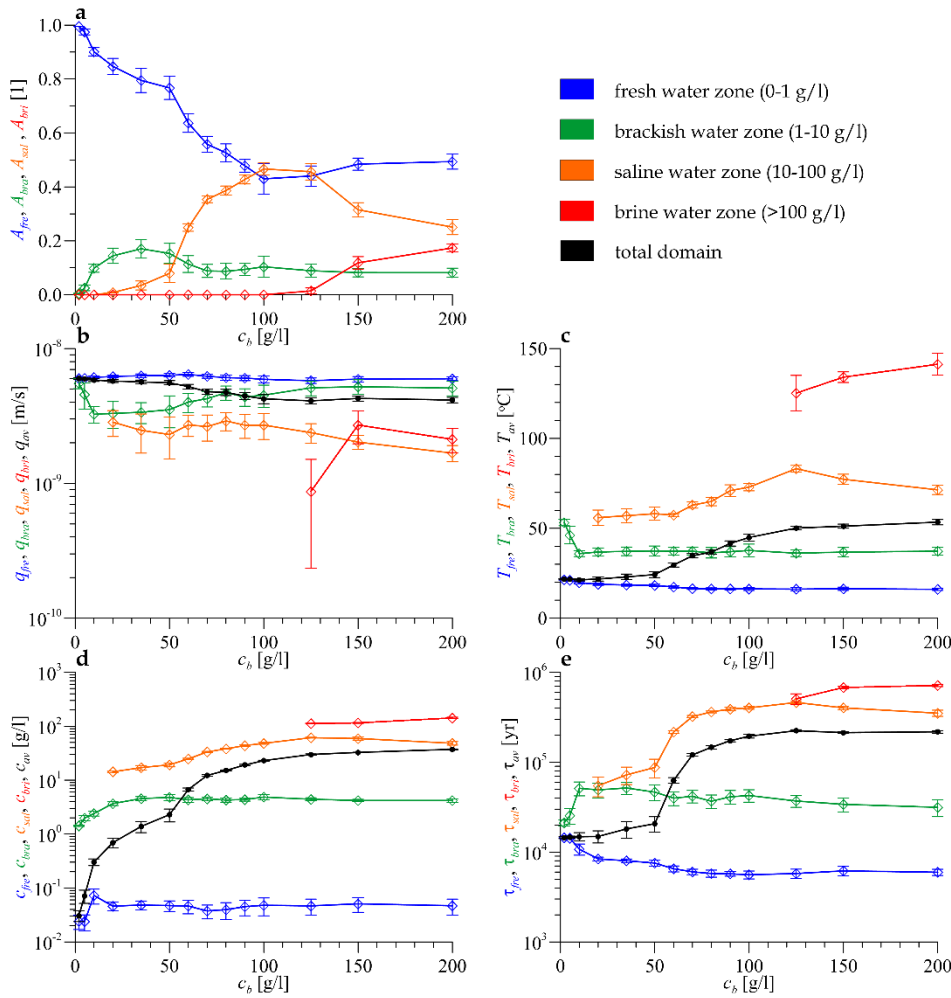
Figure 8. (a) The relative area, (b) the Darcy flux, (c) the temperature, (d) the concentration and (e) the age of the salinity zones plotted against the bottom solute concentration. Each salinity zone is marked with a different colour. The values averaged for the whole model domain are shown in black. Standard deviations calculated for the quasi-stationary phase of the time series are marked by error bars.

3.2 Topothermohaline convection in Buda Thermal Karst, Hungary

3.2.1 The Buda Thermal Karst system and its numerical model

The Buda Thermal Karst (BTK) system consists of two main parts: a predominantly unconfined and a confined carbonate system (Mádl-Szőnyi and Tóth, 2015). The two interconnected parts are bordered by the Danube River as a natural geographical margin. The uncovered karst west of the Danube includes the Buda Hills (559 asl) and the Pilis (756 asl), while the eastern side includes the Pest Plain and the Gödöllő Hills, where the topography varies between 95 and 350 asl (Fig. 9). The mean annual temperature of the Buda Thermal Karst system is 10 °C, while the annual precipitation is 500–600 mm yr^{-1} (Mersich et al., 2003).

385
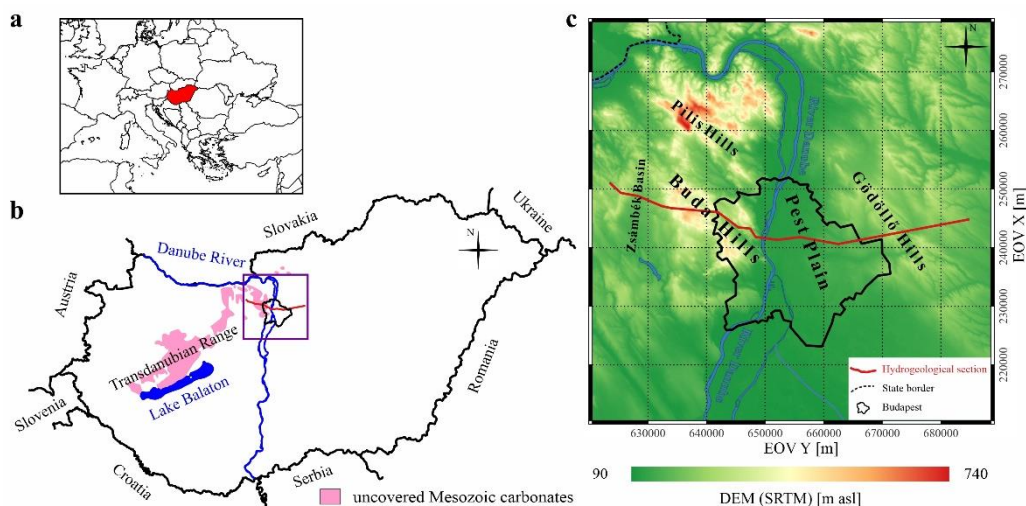
Figure 9. (a) The location of Hungary in Europe, (b) the study area with uncovered Mesozoic carbonates and (c) the topography of the study area. The hydrogeological section crossing the Buda Thermal Karst system is marked by the red line (modified after Szijártó et al. (2021)).

The western part of the BTK consists of 2–3 km thick, karstified dominantly Triassic limestone, dolomite and marl,

390 and is, therefore, the main aquifer of the area (HS8–10 in Fig. 10). The system is downfaulted to the east of the Danube and becomes confined. The carbonate complex of the BTK is overlain by siliciclastic sediments and marls from the Eocene, as well as by pelagic clays from the Oligocene (HS4–7). The latter is the main aquitard unit in the area. From the Miocene, siliciclastic sediments began to be deposited again, alternating low and high permeability layers until the present surface (HS1–3) (Mádl-Szőnyi, 2019). Figure 9 shows the trajectory of the modelled hydrogeological section crossing Budapest, the capital

395 of Hungary, and the wider geographical setting of the BTK system. Figure 10 presents the topography, the geology interpreted by Fodor (2011) and the hydrogeological conditions, including 11 hydrostratigraphic units (HS) and the simplified water table elevation (Mádl-Szőnyi et al., 2019; Szijártó et al., 2021) along the 2D section with a length of 63.8 km and average thickness of 5140 m. Table 3 summarizes the physical parameters of each unit, adapted from Szijártó et al. (2021), where the hydraulic conductivity of the layers, K is given instead of the permeability, as only these were available from the literature and well tests.

400 Minor modifications were introduced in the values of the hydraulic conductivity of HSs, since the model of Szijártó et al. (2021) applied isotropic hydraulic conductivity, whereas this model assumes a higher anisotropy ($\varepsilon=k_x/k_z=100$) for siliciclastic units (e.g. Galsa, 1997) and a lower anisotropy ($\varepsilon=10$) for carbonate units (e.g. Havril et al., 2016).
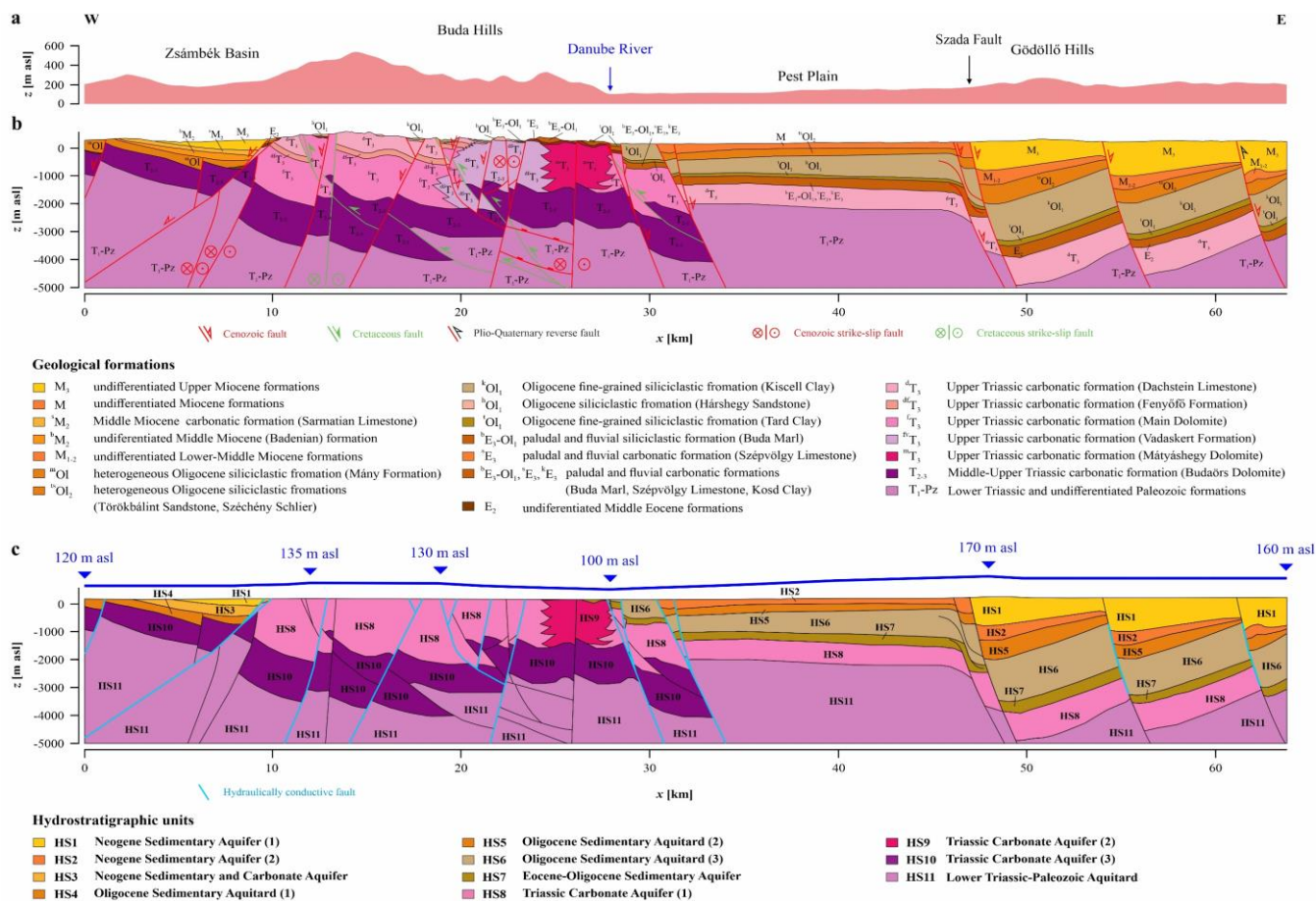
Figure 10. (a) The topography along the two-dimensional section, (b) the geological section (based on Fodor (2011)) and (c) the hydrogeological section, including the 11 HSs and the simplified water table adapted from Szijártó et al. (2021). Vertical exaggeration is 1.5.

Table 3. Parameters of hydrostratigraphic units in the Buda Thermal Karst model.

Hydrostratigraphic units	K [m s^{-1}]	ε [1]	Φ [1]	ρ_m [kg m^{-3}]	λ_m [W m^{-1} K^{-1}]	c_{pm} [J kg^{-1} K^{-1}]
HS1	10^{-5}	100	0.15	2200	1.8	840
HS2	10^{-6}	100	0.10	2200	1.8	840
HS3	10^{-6}	10	0.10	2600	2.0	900
HS4	10^{-8}	100	0.10	2500	1.8	900
HS5	10^{-7}	100	0.10	2500	1.8	900
HS6	10^{-9}	100	0.05	2000	1.5	2100
HS7	10^{-6}	100	0.15	2100	2.0	840
HS8	10^{-5}	10	0.15	2700	2.5	850

HS9	10^{-5}	10	0.15	2700	2.5	850
HS10	10^{-5}	10	0.10	2750	2.2	800
HS11	10^{-7}	10	0.10	2750	2.2	800

410   The boundary and initial conditions were chosen to be similar to those of the synthetic base model, which were certainly adapted to the specific hydrogeological situation. For the flow, no-flow boundary conditions were imposed at the lower and vertical boundaries of the model, while the topography-driven groundwater flow was driven by the gradient of the water table determined on the basis of the available data (Fig. 10.c). The lateral groundwater connection between the BTK and the surrounding hydrogeological systems is not excluded, but no observations are available to quantify this process. The initial

415   condition was a Darcy flux distribution corresponding to the reference water density. For temperature, the vertical boundaries were assumed to be insulating in the absence of significant transverse water movement, and a constant heat flux of 100 mW m^{-2} was applied along the lower boundary due to the high heat flux characterizing the area (Lenkey et al., 2021). The surface temperature was set at 10 °C due to the geography of the study area. The initial condition was a conductive temperature distribution. For salt concentration, no flux at the side boundaries and constant concentration at the lower (35 g l^{-1}) and upper

420   (0 g/l) boundaries were prescribed. As an initial condition, the concentration was uniform at 35 g l^{-1} in all hydrostratigraphic units due to the fact that each formation was deposited in a marine environment (Mádl-Szőnyi et al., 2019). This is reflected in the chosen lower boundary condition, while the upper boundary condition is the consequence of precipitation infiltration. For the water age, similar to the base model, there was no flux at all boundaries except on the surface, where the open boundary condition was applied (Eq. (7)), the water age at the beginning of the simulation was set to zero in the whole model domain.

425   Analogous to the synthetic model simulations, the numerical treatment of the BTK problem was obtained by solving the PDE system of Eqs. (1)–(5) using COMSOL Multiphysics 5.3a software. The maximum finite element size used was 100 m inside the model domain and 50 m at the outer boundaries of the model, where boundary layer elements were also used. This resulted in a total of 160 775 elements. Unknown variables inside the finite elements were approximated in the same way as for the synthetic model. At the beginning of the time-dependent simulation, the time step was increased exponentially until

430   1 kyr to handle the initial transient phenomena more accurately, and then the maximum time step was fixed at $t=20$ yr. The simulation was continued to 1 Myr, because this time scale is comparable to the geological time scale of the area, and longer calculations would have had to take geological processes into account (Havril et al., 2016). The calculation, therefore, took about 10 days of CPU time and required approx. 8 GB of memory.

3.2.2 Numerical model results of the BTK system

435   Figure 11 illustrates the evolution of the flow, temperature, solute content and water age of the Buda Thermal Karst system over 1 Myr. At 1 kyr after the start of the simulation, two types of flow regimes were developed (Fig. 11.a). (1) A topography-dominated flow regime was formed in the unconfined part of the Buda Thermal Karst system ($x=10$–27 km in HS8–10) down to a depth of 3 km, and in the uppermost Neogene aquifers on the Pest side ($x=30$–63 km in HS1–2). (2) On the other hand,

thermohaline convection developed in the deeper, saline covered carbonates (e.g. x=47–62 km in HS8). After 1 kyr, most of

440 the system is characterized by its initial state, with nearly conductive temperature distribution (Fig. 11.b) and high solute content (Fig. 11.c and d). The infiltrating young freshwater reaches only the upper few hundred meters of the near-surface permeable units (Fig. 11.c–e). For better comparisons, the water age non-dimensionalised with simulation time is shown in Fig. 11.

After 10 kyr, precipitation infiltrating through unconfined carbonates floods the karstified reservoir (HS8–10) with

445 young, cold freshwater (Fig. 11.g–j). Moreover, this water mass is already appearing in the confined reservoir, about 5 km east of the Danube River (x=32 km). At this stage, most of the confined carbonate reservoir (HS8) and the Oligocene clayey cover (HS5–6) are still saturated with warm, saline water. In the confined karsts, thermohaline convection forms in the saline pore water at x=32–62 km (Figure 11.f).

100 kyr after the start of the simulation, the flow pattern is essentially unchanged (Fig. 11.k). The size of the

450 topography-dominated flow region has increased, while the front of warm, saline and aged water associated with the confined carbonates has clearly retreated to the east (Fig. 11.l–o). The boundary of the thermal water is now 15 km east of the Danube (x=42 km), the saline water was replaced by brackish water up to the Szada Fault (x=47 km). There is a strong correlation between water age and salt concentration distribution (Fig. 11.m and o): the younger, less saline water is already present in the deepest covered carbonates (HS8: x=58 km). Thermohaline convection in the confined reservoirs effectively mixes young,

455 cold freshwater infiltrating from the west with old, warm and saline water from the east, thus facilitating the propagation of the topography-driven groundwater flow zone.

After 1 Myr, the high-temperature geothermal reservoir (T>150 °C) retreats to the deeper (>2 km) eastern zone (x>42 km) (Fig. 11.q). Moreover, thermal water with medium temperature (T=50–150 °C) is found in the western part of the confined reservoir under the clayey cover layer (HS7–8: x=27–42 km), which reaches the surface at the Danube line at the

460 confined-unconfined margin. The extent of the saline groundwater is somewhat larger, as they are found in the low permeability Oligocene covers in addition to the high-temperature geothermal reservoir (Fig. 11.s). The Oligocene clays (HS6) contain the oldest waters of the section, with an age practically equal to the duration of the simulation (1 Myr), i.e. their origin is representative of the sedimentary environment (Fig. 11.t). The cold, young, low salinity waters infiltrating from the unconfined site reach as far as the Szada Fault (x=47 km), and even result in a noticeable decrease in concentration and

465 rejuvenation of the groundwater in the karstified carbonates (HS8) up to the eastern boundary of the section (Fig. 11.r and t). In these domains, thermohaline convection is the prevailing component of groundwater flow over a long period of time (Fig. 11.p). In the Neogene sediments above the cover layer (HS1–2: x=32–63 km) and in the unconfined carbonates (HS8–10: x=10–27 km), topography-driven water flow continues to dominate, characterised by cold and young water with low solute content.

470
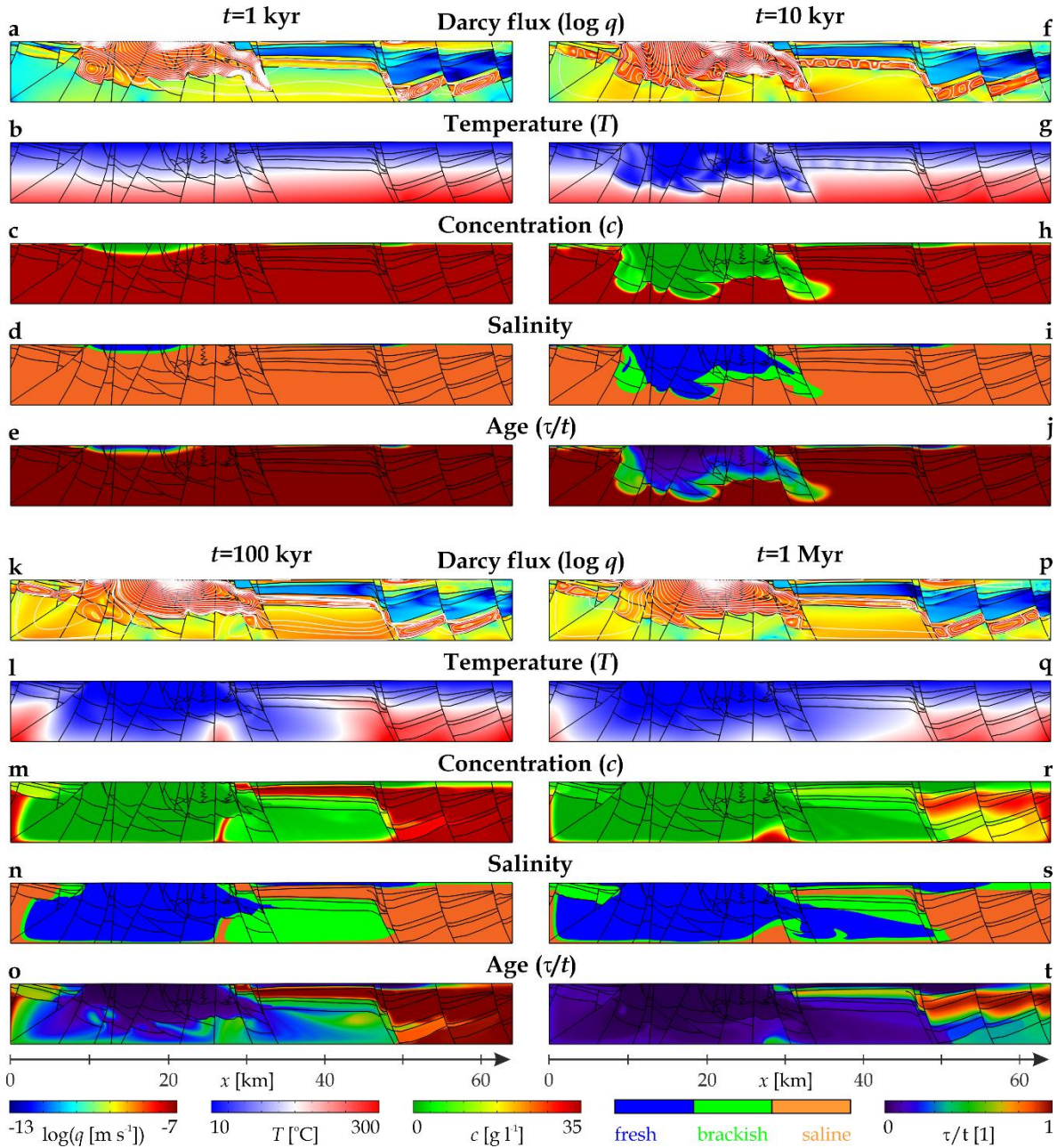
Figure 11. Evolution of the topothermohaline convection in the Buda Thermal Karst system. Distributions of (a, f, k, p) the Darcy flux, (b, g, l, q) the temperature, (c, h, m, r) the solute concentration, (d, i, n, s), the salinity zones and (e, j, o, t) the water age at different simulation times of 1 kyr, 10 kyr, 100 kyr and 1 Myr. The direction of Darcy flux is shown with streamlines (white). The water age, τ is normalized by the simulation time, t.

As concerns the Buda Thermal Karst system, it can be concluded based on the numerical model calculation that cold and young freshwater entering through unconfined karstic carbonates is effectively mixed with the warm, aged and saline water characteristic of the confined carbonate system below the Pest plain. The mixing zone propagates gradually but at a

slower rate eastwards, facilitated by thermohaline convection in the reservoir. Groundwater, mixed in temperature, chemical
480 composition and age, moves westwards within the upper part of HS8 directly beneath the Oligocene cover, transporting the
mixed water to the Danube line, the margin between the confined and unconfined carbonate system, where it reaches the
surface (Animation S8 in Galsa et al., 2025).
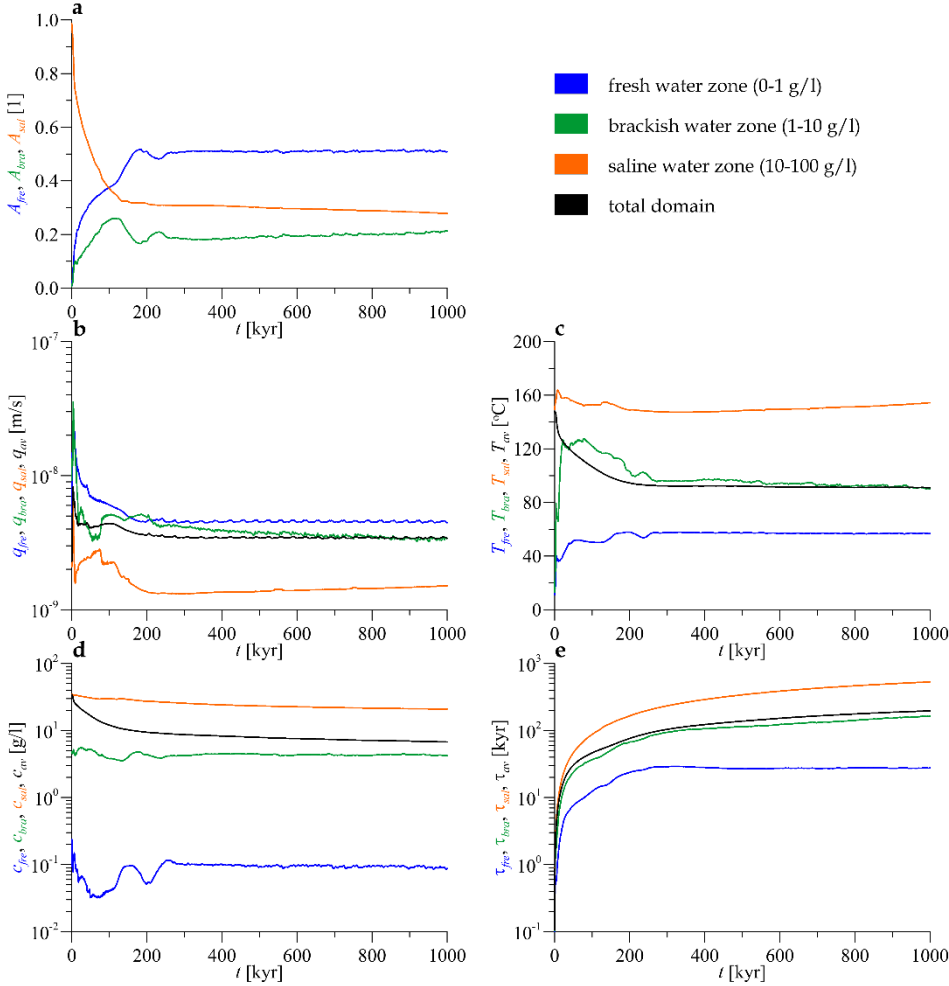
485 **Figure 12. The time series of (a) the relative area, (b) the Darcy flux, (c) the temperature, (d) the concentration and (e) the water age
of different salinity zones. The values averaged for the whole model domain are shown in black.**

Most of the time series of the control parameters shows that the BTK model reached or approached its quasi-stationary
solution after 200–300 kyr (Fig. 12). After this transient process, half of the system is saturated with freshwater (A_{fre}=51%),
490 and the relative area of the brackish water domains is slowly increasing (currently A_{bra}=21%) at the expense of the saline water
domains (A_{sal}=28%) (Fig. 12.a). The latter category includes, as illustrated in Fig. 11, the deep geothermal reservoir and the

Oligocene clay cover. The Darcy flux time series makes it clear that the solution of the problem is not stationary (Fig. 12.b). The periodicity of the flux intensity suggests that the processes in the freshwater domains in the first place and in the brackish water domains in the second place are weakly time-dependent. Their local Rayleigh numbers may slightly exceed the critical value, resulting in weak, periodic thermal convection in the deepest part of the unconfined carbonates and thermohaline convection in the confined carbonates (Animation S8 in Galsa et al., 2025). The saline, brackish and freshwater regions are clearly distinct in terms of flow intensity, temperature and age (Fig. 12.b, c and e). The saline zones are characterised by slow flow ($q_{sal}=1.5 \cdot 10^{-9}$ m s^{-1}), high temperature ($T_{sal}=154$ °C) and high water age ($\tau_{sal}=530$ kyr). These regions saturated with saline and brackish water have not completely reached the quasi-stationary state even after 1 Myr. In contrast, freshwaters, directly connected to precipitation, have a higher and time-varying Darcy flux ($q_{fre}\approx4.4 \cdot 10^{-9}$ m s^{-1}), but lower temperature ($T_{fre}=57$ °C) and age ($\tau_{fre}=27.5$ kyr). Based on the control parameters, the most marked differences between the saline and freshwater domains are in solute concentration (factor of 240) and age (factor of 19.3). These parameters seem to be the most sensitive for the separation of the different zones (Fig. 12.d and e).

4 Discussion

We performed a two-dimensional synthetic simulation set to assess the interaction of topography-driven forced convection and free thermal and haline convection on the groundwater flow. In the studied base model (Tables 1 and 2), two flow domains are separated, the recharge and transition zones are dominated by topography-driven regional water flow, and the domain is characterised by young, cold freshwater. The emerging warm and brackish upwellings are driven by regional flow towards the discharge zone. However, a thermohaline dome develops beneath the discharge zone, in which free thermohaline convection is the dominant flow regime with warm, saline and aged waters (Fig. 2).

The reduction of the hydraulic gradient strengthens the thermohaline flow regime, which, in fact, floods the entire basin at low water amplitude ($H \leq 20$ m). In a narrow interval ($H=20–100$ m), the role of the thermohaline flow regime is strongly reduced, and in the models of $H=200–500$ m, the influence of regional flow is clearly dominant over most of the basin ($A_{fre}>95\%$). This sweeps warm, saline, aged waters out of the model domain, and also results in a near steady-state solution (Fig. 3). For these simulations, ignoring free thermohaline convection would only lead to minor inaccuracies in the solutions.

The variation of the bottom heat flux affects the behaviour of the coupled flow system directly through the temperature. It is not evident that in the model of $q_{Tb}=90$ mW m^{-2}, the extension of the thermohaline dome is at its maximum ($A_{sal}=35\%$), and the average temperature is at its highest ($T_{av}=35$ °C). A higher bottom heat flux induces such intense thermal convection that it leads to a weakening/disappearance of the thermohaline dome and reduces the average temperature of the basin paradoxically (Fig. 5 and 6).

At low bottom salt concentrations, the flow in the basin is controlled by the topography of the water table, which is perturbed by buoyant thermal upwellings (Fig. 7). In models with $c_b \leq 20$ g l^{-1}, a large part of the basin is saturated by freshwater ($A_{fre}>80\%$), resulting in low average temperature ($T_{av}<22$ °C) and young water ($\tau_{av}=15$ kyr). Increasing c_b moderates the flow

and forms a dome with multilayer thermohaline convection beneath the discharge zone. This is accompanied by temperature
525 and water age increases of more than 30 °C and one order of magnitude, respectively.

Simple (two-dimensional, homogeneous and isotropic) synthetic model calculations draw attention to the fact that the final state of the interconnected processes in nature is, in most cases, not predictable. While the effect of changing some parameters can be qualitatively inferred (e.g. increasing the amplitude of the water table enhances the dominance of topography-driven groundwater flow), quantification is only possible on the basis of numerical, possibly analytical,
530 calculations. In addition, there are complex relationships in the coupled problem whose effect is not even qualitatively evident (increasing heat flux decreases average temperature). In this context, it can be concluded that the numerical simulations should be carried out by building the most general model possible, of course, after compromising with the available computational resources. This will ensure that the subjectivity of the numerical modeller has the least possible influence on the final results of the calculations. However, depending on the hydrogeological and geothermal conditions of the area, certain phenomena and
535 physical processes can be ignored, but their negligibility must always be confirmed by a series of comprehensive preliminary simulations.

The operation of the topothermohaline convection model was demonstrated in a real hydrogeological situation in the Buda Thermal Karst area of Hungary. The numerical solution suggests that the western, uncovered karst is filled up by cold, young freshwater infiltrating from precipitation in as short as 10 kyr (Fig. 11.f–j). Here, the topography-driven forced
540 convection is the dominant driving force, apart from warm upwellings evolving in the deepest parts of the system. However, groundwater with higher temperature and salinity in the eastern confined karst may persist over geological time scales, at least in the more confined eastern zones of the reservoir (Fig. 11. p–t). In these confined but highly permeable regions, free thermohaline convection develops, actively transporting warm, solute-rich and aged waters towards the main outflow zone, the Danube River. Thus, waters of different temperature, chemical composition and age from the western unconfined karst and
545 the eastern confined karst and its cover are effectively mixing under the western part of the Pest Plain, contributing to the karstification process (Erőss et al., 2008; 2012; Erőss, 2010; Licour, 2014).

This picture is strongly analogous to the flow-temperature-salinity system in the Tiberias Basin revealed by the numerical simulations of Magri et al. (2015), although that area is characterised by significantly lower heat flux (60 mW m^{-2}) but higher TDS content (up to 300 g l^{-1}) and different geological build-up. The near-surface Quaternary and Tertiary
550 complexes are dominated by topography-driven regional groundwater flow with low temperature and salinity, while thermohaline convection is formed in the deeper and more confined Mesozoic carbonates of the Golan Heights. The connection of the latter to the surface is through high-permeability faults, which explains the higher temperatures and TDS contents in springs and wells around Lake Tiberias. Zech et al. (2016) studied the coupled phenomenon of groundwater flow, heat and mass transport in the Thuringian Basin. They found that free thermohaline convection has a minor role in the hydrogeological
555 situation, which is not surprising considering the shallow (1 km deep) basin with a temperature difference of only 30 °C. However, the Zechstein salt deposit, which forms the reservoir bed, causes a 20% density increase over the entire basin depth, substantially exceeding the destabilising effect of thermal convection. Kaiser et al. (2013b) investigated the effect of salt

diapirism and the incomplete clayey cover layer (hydrogeological window) separating partially the two aquifers on the resulting topothermohaline convection in the Northeast German Basin. It was concluded that the hydrogeological window favours advective heat and mass transport, i.e. the topography-driven water flow regime. However, thermal buoyancy locally (outside the salt domes in the covered reservoir) can overcome the effect of stabilizing haline buoyancy. As a consequence, 'deep-seated buoyant groundwater circulates upward transporting heat and mass to shallower levels within the Upper Saline Aquifer' (Kaiser et al., 2013b). Nevertheless, for the last two models, it should be noted that the water table was adjusted to the surface, and thus — presumably — amplified the effect of topography-driven forced convection at the expense of free thermohaline convection.

In the case of BTK, lukewarm springs in uncovered karst areas are mainly characterised by intermediate temperature (20–28 °C), low chloride content (10–40 mg l^{-1}) and high yield (>1800 l min^{-1}). However, as the margin of the uncovered-covered karst is approached, thermal springs (38–58 °C, >80 mg l^{-1}, <600 l min^{-1}) appear. The analysis of the chemical composition of the spring waters clearly indicates a discharge of ~~two~~ different types of water (Kovács and Erőss, 2017; Mádlné Szőnyi et al., 2018; Mádl-Szőnyi, 2019). TDS data from wells show a general increasing trend from west to east. While the unconfined karst waters always fall into the freshwater category (c<1 g l^{-1}), the TDS of the confined waters on the eastern side presents a more complex pattern. The saline waters (>10 g l^{-1}) sampled in the clayey Oligocene cover (HS5–6) are at their maximum, with TDS values occasionally reaching 40–50 g l^{-1} (Mádl-Szőnyi et al. 2019). It is observed that the higher concentration values are related to the thickening of the aquitard, indicating the dominance of diffuse mass transport (cf. Fig. 11.r) and suggesting the presence of sedimentary saline marine water. However, water samples from the confined karst show the presence of fresh or brackish water (<10 g l^{-1}), and only the most easterly, more confined areas contain saline water. The origin of these waters is probably mixed and may include karstic fresh waters, as well as waters with higher salinity from the aquitards above and below. This is in full agreement with the numerical results presented.

New geothermal projects in the BTK area generally target fresh or brackish thermal waters with a moderate temperature (50–80 °C) in the western part of the shallower, confined karst (HS7 and 8: x=27–42 km). This is fully consistent with the numerical model of westward groundwater flow under the Oligocene clayey cover, which transports the groundwater having mixed chemical composition, temperature and age from the eastern reservoir (Fig. 11.p). Temperature-elevation profiles in many areas reveal significant deviations from the average geotherm, sometimes with decreasing temperatures with depth (Mádl-Szőnyi 2019). This can indicate the presence of significant vertical advection and/or free thermal convection, which in complex karst systems can reduce the probability of success of a geothermal project and increase the vulnerability of the aquifer (Tóthi et al., 2024). Nevertheless, it highlights the significant geothermal potential of the upper Triassic Dachstein Limestone (HS8) and Eocene (HS7, e.g. Szépvölgyi Limestone) reservoirs in the eastern part of the BTK (Fig. 10.b), which is of higher temperature but greater depth, according to our numerical simulations.

In the BTK model, the role of faults was not investigated in this study. Faults appearing in Figure 10 represent only the boundaries of individual hydrostratigraphic/geometric units without physical parameters. However, Szijártó et al. (2021) studied the effect of the conduit faults on heat transport and recharge rate in the mixed (topography- and thermal buoyancy-

driven) convection regime of BTK. They established that conduit faults enhanced the Nusselt number by 21%, while reduced the recharge rate by 10%, resulting in rather local anomalies in temperature and flow pattern similarly to findings of Przybycin et al. (2017), Zech et al. (2016) and Czauner et al. (2024), etc. Such hydraulically conducting channels, especially on the eastern side of the reservoir, would facilitate the upwelling of warm, aged and saline waters as observed by Magri et al. (2015) around Lake Tiberias. However, only at the deepest central margin of unconfined and confined karst areas of BTK do these faults cause surface manifestations in temperature and salinity of springs.

Szijártó et al (2054) studied the water age of the BTK system in a geologically simplified two- and three-dimensional numerical model. They found that the calculated water age in the confined reservoir, especially in its eastern and deeper regions, increases by orders of magnitude (τ>100 kyr, in some cases >1 Myr) compared to the shallower regions of the unconfined area (τ=0–10 kyr), in full agreement with the results presented here. This is partly supported by the highly sporadic records of ^{14}C ages of water samples from springs, caves and thermal wells. The ages of spring waters in uncovered areas show approximate values of 5 kyr, while the ages of waters from the depth range of 1000–1600 m suggest values of 15–25 kyr (Deák, 1979; Fórizs et al., 2019). Our numerical model results are consistent with the water ages measured in the shallow and uncovered areas but produce somewhat higher water ages in the deeper zones (~50 kyr). Overall, Balderer et al (2014), based on [36]Cl/Cl ratio data, can reflect equilibrium conditions and long (~million years) residence time. They propose the possibility of mixing with "very old" groundwater components.

Of course, like all models, the present simulations apply approximations too. Although the dependence of the water density on temperature, pressure and salinity in the buoyancy was taken into account, the effect of these parameters on the viscosity of the water was neglected. Based on our preliminary calculations, the effect of temperature on viscosity is the dominant factor that promotes transport processes in the deeper, warmer regions, thus increasing the intensity of thermohaline convection in confined reservoirs. Meanwhile, in the unconfined zones, low temperature slightly moderates the flow intensity due to enhanced viscosity. Another question may arise regarding the lower boundary condition for salt concentration. Unfortunately, we do not have geological information on the hydrogeological conditions beneath the Lower Triassic-Paleozoic Aquitard (HS11). In this study, the simplest lower boundary condition consistent with the initial condition (marine sedimentation environment) was chosen, the salt concentration was kept constant, c_b=35 g l^{-1}. At the same time, the salinity of the presumably low permeability region below the BTK may be reduced, and the salt may partially diffuse towards the aquifers, from where it may be transported by topothermohaline convection. Thus, a simulation with a modified boundary condition was carried out, in which a 1 km thick impermeable layer was added beneath the BTK model and a constant concentration of c_b=35 g l^{-1} was prescribed at the bottom. New model calculation including both temperature-, pressure- and concentration-dependent viscosity as well as the lower impermeable layer is presented in the Supplementary material. It can be concluded that salt concentration is reduced in the deep confined part of the BTK system as a consequence of (1) more intense advection due to decreased temperature-dependent viscosity and (2) retained salt transport through the diffuse impermeable lower layer. As a result, younger waters appeared in the confined deep reservoir. However, the main characteristics of flow/temperature/salinity/water age, such as topography-driven flow in the unconfined karst, thermohaline convection in the

confined karst, high geothermal potential in the eastern reservoir, elevated salt concentration in the clayey cover etc., have not been changed.

In synthetic simulations, the effect of mechanical dispersion was not taken into account to focus on the phenomenon of topothermohaline convection (Table 1). Test calculations indicate that (1) transverse dispersion facilitates salt transport 630 through the bottom boundary and (2) longitudinal dispersion promotes mixing within the thermohaline dome, enlarging its size, which results in higher average salt concentration, temperature and water age, but lower Darcy flux (Supplementary material). The process is identical to that studied in detail in the topohaline (topography-driven and free haline) convection models of Galsa et al. (2022).

The two-dimensional approach obviously reduces the degree of freedom of the system, although the 3D treatment of 635 the phenomenon is not yet feasible with the available computing capabilities (1–2 weeks CPU time for one simulation in 2D). Nevertheless, two-dimensional simulation is an effective way to facilitate the preliminary investigation of real hydrogeological problems and to draw attention to the complexity of the phenomenon and the interaction of the different forces driving groundwater flow.

Around 10% of current worldwide geothermal energy production is related to extensional domain type geothermal 640 plays, which are typically deep sedimentary basins characterised by an elevated heat flow (Moeck, 2014; Moeck and Beardsmore, 2014; Moeck et al., 2015). As these represent a prospective target for future geothermal developments, the understanding of the hydrogeological processes of these regions would require the analysis of multiple coupled driving forces, such as water table undulation (by topography), temperature (by high heat flux) and salinity differences (by sedimentation processes). Therefore, the application of the topothermohaline convection model could be potentially extended to Western 645 Anatolia (Turkey) (Gokgoz et al., 2010; Özkaymak and Sözbilir, n.d; Özler, 2000), the East African Rift System in Uganda (Kato, 2016) and Kenya (Otieno, 2020), the Rhine Graben (Europe) (Rybach, 2007; Schindler et al., 2010), Mexico (Gutierrez-Negrin, 2015; Prol-Ledesma and Morán-Zenteno, 2019) and the Great Basin region (Western USA) (Faulds et al., 2010; Faulds et al., 2006; Siler and Faulds, 2013).

5 Summary and conclusions

650 Two-dimensional numerical model calculations were performed to reveal the combined effects of topography-driven forced convection and temperature- and salinity-driven free thermal and haline convection on the basin-scale groundwater flow. In the first step, we analysed the influence of the amplitude of the groundwater table, the bottom heat flux and salt concentration on the flow pattern, temperature, solute content and water age distribution in a synthetic homogeneous model domain. All of the factors investigated significantly affect the control parameters, and the simulations lead to a time-dependent quasi-655 stationary solution with a dynamic equilibrium between topography-driven forced convection, positive thermal and negative haline buoyancy. We conclude that

- in the base model (H=50 m, q_{Tb}=90 mW m^{-2}, c_b=70 g l^{-1}), the recharge zone and the central regions of the basin are dominated by topography-driven regional groundwater flow, with low average temperature, salinity and water age. While below the discharge zone, a dome with high temperature, salinity and water age develops, in which vigorous thermohaline convection is formed.

- Decreasing the amplitude of the water table reduces the hydraulic driving force and, thus, facilitates the extension of the thermohaline dome, which can eventually flood most of the basin. In contrast, increasing the water table amplitude intensifies the topography-driven regional water flow, which effectively sweeps heat, solute content and aged water out of the system. This shifts the time-dependent solution towards a stationary final state.

- The decrease in the bottom heat flux reduces the thermal buoyancy, thus the extent of the thermohaline dome, the flow intensity and the average temperature. Increasing the heat flux, on the other hand, strengthens the thermal buoyancy and, thus the intensity of the water flow, which also leads to a decrease in the average temperature and the rejuvenation of the groundwater.

- The decrease in salt concentration at the bottom boundary weakens the role of negative haline buoyancy, resulting in the dominance of topography-driven flow, perturbed by warm upwellings drifting towards the discharge zone. Increasing salt concentration restrains regional flow and promotes the development of a multilayered thermohaline dome, which significantly enhances both the average temperature and the water age in the basin.

The physical understanding of the combinations of driving forces sheds light on the complex processes that control flow in groundwater basins. It highlights (i) the large variations in temperature, salinity and water age as a result of topothermohaline convection, even in homogeneous basins; (ii) the importance of understanding the fluid evolution history of sedimentary basins based on the time-dependence of these processes, and (iii) the often oversimplified flow interpretations derived from sporadic water chemistry or isotopic data.

The phenomenon of topothermohaline convection was demonstrated along a real two-dimensional section crossing the Buda Thermal Karst, Hungary. The section is divided into two areas with different characters by the Danube River. West of the Danube, karstified carbonates are mostly unconfined, while east of the Danube, they are covered by the Oligocene clayey and Neogene sediments. Consequently, numerical model results show that

- in the western unconfined area, as little as 10 kyr is sufficient to saturate a large part of the karstified carbonates with infiltrating cold, young, fresh precipitation. The flow is primarily controlled by the topography of the groundwater table, only in the deepest parts of the basin do warm upwellings develop and drift towards the Danube as the main discharge zone.

- In contrast, in the deep and confined karst reservoir of the eastern side, high temperatures, salinity and water age can persist over geological timescales (>1 Myr), making the area a prime target for future geothermal exploration. Thermohaline convection forms in the covered carbonates, transporting hot, saline and aged waters toward the Danube.

690 ▪ Between the two areas, but already in the confined part, a mixing zone is formed. The mixed temperature and chemistry of the groundwater contribute to the evolution of karstification in the confined reservoir and explain the difference between the surface lukewarm and warm springs as well as the temperature distribution in the thermal wells.

The gradual increase in geological and geophysical observations from the BTK site will allow the model to be fine-

695 tuned, and, thus the parameters of the covered geothermal reservoir on the eastern side to be more accurately determined.

Data availability

No data sets were used in this article

Author contributions

AG: conceptualization, investigation, methodology, ~~investigation,~~ resources, validation, visualization, writing – original draft,

700 writing – review & editing. MSz: data curation, funding acquisition, resources, supervision, visualization, writing – review & editing. ÁT: data curation, supervision, writing – review & editing. JM-Sz: data curation, conceptualization, funding acquisition, supervision, writing – review & editing.

Competing interest

The authors declare that they have no conflict of interest.

705 ### Acknowledgements

The research was funded by the National Multidisciplinary Laboratory for Climate Change, RRF-2.3.1-21-2022-00014 project and by the National Research, Development and Innovation Office in the framework of project No. PD 142660.

References

An, R., Jiang, X.-W., Wang, J.-Z., Wan, L., Wang, X.-Z., and Li, H.: A theoretical analysis of basin-scale groundwater temperature distribution, Hydrogeology Journal, 23, 397–404, https://doi.org/10.1007/s10040-014-1197-y, 2015.

Bagheri, R., Nadri, A., Raeisi, E., Kazemi, G.A., Eggenkamp, H.G.M., and Montaseri, A.: Origin of brine in the Kangan gasfield: isotopic and hydrogeochemical approaches, Environmental Earth Sciences, 72, 1055–1072, https://doi.org/10.1007/s12665-013-3022-7, 2014.

Balderer, W., Synal, A.H., Deák, J., Fórizs, I., and Leuenberger, F.: Origin of thermal waters in Budapest based on chemical and isotope investigations including chlorine-36, in: Balderer, W., Porowski, A., Idris, H., LaMoreaux, J. (eds), Thermal and Mineral Waters, Environmental Earth Sciences. Springer, Berlin, Heidelberg, https://doi.org/10.1007/978-3-642-28824-1_5, 2014.

Barlow, P.M. and Reichard, E.G.: Saltwater intrusion in coastal regions of North America, Hydrogeology Journal, 18, 247–260, https://doi.org/10.1007/s10040-009-0514-3, 2010.

Birkle, P., García, B.M., and Padrón, C.M.M.: Origin and evolution of formation water at the Jujo–Tecominoacán oil reservoir, Gulf of Mexico. Part 1: Chemical evolution and water–rock interaction, Applied Geochemistry, 24, 543–554, https://doi.org/10.1016/j.apgeochem.2008.12.009, 2009.

Bredehoeft, J.D.: The Toth revolution, Groundwater, 56 (1), 157–159, https://doi.org/10.1111/gwat.12592, 2018.

Bresciani, E., Gleeson, T., Goderniaux, P., de Dreuzy, J.R., Werner, A.D., Wörman, A., Zijl, and W., Batelaan, O.: Groundwater flow systems theory: research challenges beyond the specified-head top boundary condition, Hydrogeology Journal, 24, 1087–1090, https://doi.org/10.1007/s10040-016-1397-8.

Clauser, C., and Villinger, H.: Analysis of conductive and convective heat transfer in a sedimentary basin, demonstrated for the Rheingraben. Geophysical Journal International, 100 (3), 393–414, https://doi.org/10.1111/j.1365-246X.1990.tb00693.x, 1990.

Conlon, T.D., Wozniak, K.C., Woodcock, D., Herrera, N.B., Fisher, B.J., Morgan, D.S., Lee, K.K., and Hinkle, S.R.: Ground-Water Hydrology of the Willamette Basin, Oregon, USGS, Scientific Investigations Report 2005–5168, pp. 83, https://pubs.usgs.gov/sir/2005/5168/pdf/sir2005-5168.pdf, 2005.

Cserepes, L., and Lenkey, L.: Forms of hydrothermal and hydraulic flow in a homogeneous unconfined aquifer, Geophysical Journal International, 158 (2), 785–797, https://doi.org/10.1111/j.1365-246X.2004.02182.x, 2004.

Czauner, B., and Mádl-Szőnyi, J.: The function of faults in hydraulic hydrocarbon entrapment: Theoretical considerations and a field study from the Trans-Tisza region, Hungary, AAPG Bulletin, 95 (5), 795–811, https://doi.org/10.1306/11051010031, 2011.

Czauner, B., Molnár, F., Masetti, M., Arola, T., and Mádl-Szőnyi, J.: Groundwater flow system-based dynamic system approach for geofluids and their resources, Water, 14 (7), paper:1015, https://doi.org/10.3390/w14071015, 2022.

Czauner, B., Szijártó, M., Sztanó, O., Mahrez, H.B., Molson, J., Oláh, S., and Mádl-Szőnyi, J.: Re-interpreting renewable and non-renewable water resources in the over-pressured Pannonian Basin, Scientific Reports, 14, paper: 24586, https://doi.org/10.1038/s41598-024-76076-8 , 2024.

de Hoyos, A., Viennot, P., Ledoux, E., Matray, J.-M., Rocher, M., and Certes, C.: Influence of thermohaline effects on groundwater modelling – Application to the Paris sedimentary Basin, Journal of Hydrology, 464–465, 12–26, https://doi.org/10.1016/j.jhydrol.2012.06.014, 2012.

Deák, J.: Environmental isotopes and water chemical studies for groundwater research in Hungary, International symposium on isotope hydrology (1978): Neuherberg/München, Germany, IAEA-SM-228/13, 221–247, https://inis.iaea.org/collection/NCLCollectionStore/_Public/10/460/10460882.pdf, 1979.

Deming, D.: Introduction to Hydrogeology, McGraw Hill, New York, pp. 480, ISBN-10: 0072326220, 2002.

Duffy, C.J., and Al-Hassan, S.: Groundwater circulation in a closed desert basin: Topographic scaling and climatic forcing, Water Resources Research, 24 (10), 1675–1688, https://doi.org/10.1029/WR024i010p01675, 1988.

Easteal, A.J., Price, W.E., and Woolf, L.A.: Diaphragm cell for high-temperature diffusion measurements, Journal of the Chemical Society: Faraday Transactions 1, 85 (5), 1091–1097, https://doi.org/10.1039/F19898501091, 1989.

Elder, J.W.: Steady free convection in a porous medium heated from below, Journal of Fluid Mechanics, 27 (1), 29–48, https://doi.org/10.1017/S0022112067000023, 1967.

Erőss, A., Csoma, É.A., Mádl-Szőnyi, J., Sasowsky, I., Feazel, C., Mylorie, J., Palmer, A., and Palmer, M.: The effects of mixed hydrothermal and meteoric fluids on karst reservoir development, Buda Thermal Karst, Hungary. Karst from recent to reservoirs, Karst Waters Institute, Special Publication, 14, 57–63, Google Scholar, 2008.

Erőss, A., Mádl-Szőnyi, J., and Csoma, A.É.: Hypogenic karst development in a hydrogeological context, Buda Thermal Karst, Budapest, Hungary, Groundwater quality sustainability, IAH selected papers on hydrogeology, 17, 119–133, Google Scholar, 2012.

Erőss, A.: Characterization of fluids and evaluation of their effects on karst development at the Rózsadomb and Gellért Hill, Buda Thermal Karst, Hungary, PhD Dissertation, Eötvös Loránd University, Budapest, Google Scholar, 2010.

Fabiani, G., Klaus, J., and Penna, D.: The influence of hillslope topography on beech water use: a comparative study in two different climates, Hydrology and Earth System Sciences, 28, 2683–2703, https://doi.org/10.5194/hess-28-2683-2024, 2024.

Faulds, J., Coolbaugh, M., Bouchot, V., Moeck, I., and Oguz, K.: Characterizing structural controls of geothermal reservoirs in the Great Basin, USA, and western Turkey: Developing successful exploration strategies in extended terranes, Proceedings World Geothermal Congress, Google Scholar, 2010.

Faulds, J.E., Coolbaugh, M.F., Vice, G.S., and Edwards, M.L.: Characterizing structural controls of geothermal fields in the northwestern Great Basin: A progress report, Geothermal Resources Council Transactions, 30 69–76, Google Scholar, 2006.

775   Ferguson, G., McIntosh, J.C., Jasechko, S., Kim, J.-H., Famiglietti, J.S., and McDonnell, J.J.: Groundwater deeper than 500 m contributes less than 0.1% of global river discharge, Communications Earth & Environment, 4, paper: 48, https://doi.org/10.1038/s43247-023-00697-6, 2023.

Fodor, L.: Geological sections across Budapest E-W, In: Mindszenty, A. (Ed.), Budapest: Geological Values and Man – Urbangeological Studies (in Hungarian), Eötvös Loránd University Press, Budapest, p. 20 (2013), ISBN: 9789632843681.

780   Google Scholar, 2011.

Fórizs, I., Szabó, V.R., Deák, J., Hałas, S., Pelc, A., Trembaczowski, A., and Lorberer, Á.: The origin of dissolved sulphate in the thermal waters of Budapest inferred from stable S and O isotopes, Geosciences, 9 (10), paper: 433, https://doi.org/10.3390/geosciences9100433, 2019.

Freeze, R.A., and Witherspoon, P.A.: Theoretical analysis of regional groundwater flow: 2. Effect of water-table configuration

785   and subsurface permeability variation, Water Resources Research, 3 (2), 623–634, https://doi.org/10.1029/WR003i002p00623, 1967.

Galsa, A., Herein, M., Szijártó, M., Süle, B., and Lenkey, L.: From mantle convection to groundwater flow modelling: In memoriam Prof. László Cserepes (1952–2002), Magyar Geofizika, 63 (4), 158–169, https://epa.oszk.hu/03400/03436/00256/pdf/EPA03436_geofizika_2022_4_158-169.pdf, 2022a.

790   Galsa, A., Szijártó, M., Tóth, Á., and Mádl-Szőnyi, J.: Topothermohaline convection – from synthetic simulations to reveal processes in a thick geothermal system (Supplementary material), https://dataverse.nl/privateurl.xhtml?token=b9787f3f-51ad-4aaf-a738-5a1a19e263f9, 2025.

Galsa, A., Tóth, Á., Szijártó, M., Pedretti, D., and Mádl-Szőnyi, J.: Interaction of basin-scale topography- and salinity-driven groundwater flow in synthetic and real hydrogeological systems, Journal of Hydrology, 609, paper: 127695,

795   https://doi.org/10.1016/j.jhydrol.2022.127695, 2022b.

Galsa, A.: Modelling of groundwater flow along a section in the Great Hungarian Plain using hydraulic heads measured in wells, Magyar Geofizika 38 (4), 245–256, http://epa.oszk.hu/03400/03436/00151/pdf/EPA03436_magyar_geofizika_1997_04_245-256.pdf, 1997.

Gleeson, T., and Manning, A.H.: Regional groundwater flow in mountainous terrain: Three-dimensional simulations of

800   topographic and hydrogeologic controls, Water Resources Research, 44, paper: W10403, https://doi.org/10.1029/2008WR006848, 2008.

Gokgoz, A., Yilmazli, I.E., Gungor, I., and Yavuzer, I.: Hydrogeology and environmental study at the Karahayit geothermal field (Western Turkey), Proceedings world geothermal congress, 1–7, Google Scholar, 2010.

Goode, D.J.: Direct simulation of groundwater age, Water Resources Research, 32 (2), 289-296,

805   https://doi.org/10.1029/95WR03401, 1996.

Graham, M.D., and Steen, P.H.: Plume formation and resonant bifurcations in porous-media convection, Journal of Fluid Mechanics, 272, 67–90, https://doi.org/10.1017/S0022112094004386, 1994.

Gupta, I., Wilson, A.M., and Rostron, B.J.: Groundwater age, brine migration, and large-scale solute transport in the Alberta Basin, Canada, Geofluids, 15, 608–620, https://doi.org/10.1111/gfl.12131, 2015.

810 Gutierrez-Negrin, L.C.: Cerro Prieto, Mexico — a convective extensional geothermal play, Geothermal Resources Council Transactions, 39, Google Scholar, 2015.

Haitjema, H.M., and Mitchell-Bruker, S.: Are water tables a subdued replica of the topography?, Groundwater, 43 (6), 781–786, https://doi.org/10.1111/j.1745-6584.2005.00090.x, 2005.

Havril, T., Molson, J.W., and Mádl-Szőnyi, J.: Evolution of fluid flow and heat distribution over geological time scales at the
815 margin of unconfined and confined carbonate sequences – A numerical investigation based on the Buda Thermal Karst analogue, Marine and Petroleum Geology, 78, 738–749, https://doi.org/10.1016/j.marpetgeo.2016.10.001, 2016.

Havril, T., Tóth, Á., Molson, J.W., Galsa, A., and Mádl-Szőnyi, J.: Impacts of predicted climate change on groundwater flow systems: Can wetlands disappear due to recharge reduction?, Journal of Hydrology, 563, 1169–1180, https://doi.org/10.1016/j.jhydrol.2017.09.020, 2018.

820 Hayashi, M., van der Kamp, G., and Rosenberry, D.O.: Hydrology of prairie wetlands: Understanding the integrated surface-water and groundwater processes, Wetlands, 36 (Suppl 2), 237–254, https://doi.org/10.1007/s13157-016-0797-9, 2016.

Hewitt, D.R., Neufeld, J.A., and Lister, J.R.: High Rayleigh number convection in a three-dimensional porous medium, Journal of Fluid Mechanics, 748, 879–895, https://doi.org/10.1017/jfm.2014.216, 2014.

Hussain, M.S., Abd-Elhamid, H.F., Javadi, A.A., and Sherif, M.M.: Management of seawater intrusion in coastal aquifers: A
825 review, Water, 11 (12), paper: 2467, https://doi.org/10.3390/w11122467, 2019.

Ingebritsen, S.E., Sanford, W.E., and Neuzil, C.E.: Groundwater in Geologic Processes, Cambridge University Press, pp. 536, https://doi.org/10.1017/9780511807855, 2006.

Jiang, X.-W., Cherry, J., and Wan, L.: Flowing wells: terminology, history and role in the evolution of groundwater science, Hydrology and Earth System Sciences, 24, 6001–6019, https://doi.org/10.5194/hess-24-6001-2020, 2020.

830 Jiang, X.-W., Wan, L., Wang, X.-S., Ge, S., and Liu, J.: Effect of exponential decay in hydraulic conductivity with depth on regional groundwater flow, Geophysical Research Letters, 36, paper: L24402, https://doi.org/10.1029/2009GL041251, 2009.

Jiang, X-W., Wang, X.-S., Wan, L., and Ge, S.: An analytical study on stagnation points in nested flow systems in basins with depth-decaying hydraulic conductivity, Water Resources Research, 47, paper: W01512,
835 https://doi.org/10.1029/2010WR009346, 2011.

Jiang, W., Sheng, Y., Shi, Z., Guo, H., Chen, X., Mao, H., Liu, F., Ning, H., Liu, N., and Wang, G.: Hydrogeochemical characteristics and evolution of formation water in the continental sedimentary basin: A case study in the Qaidam Basin, China, Science of the Total Environment, 957, paper: 177672, https://doi.org/10.1016/j.scitotenv.2024.177672, 2024.

Kaiser, B.O., Cacace, M., and Scheck-Wenderoth, M.: 3D coupled fluid and heat transport simulations of the Northeast
840 German Basin and their sensitivity to the spatial discretization: different sensitivities for different mechanisms of heat transport, Environmental Earth Sciences, 70, 3643–3659, https://doi.org/10.1007/s12665-013-2249-7, 2013a.

Kaiser, B.O., Cacace, M., and Scheck-Wenderoth, M.: Quaternary channels within the Northeast German Basin and their relevance on double diffusive convective transport processes: Constraints from 3-D thermohaline numerical simulations, *Geochemistry, Geophysics, Geosystems*, 14 (8), 3156–3175, https://agupubs.onlinelibrary.wiley.com/doi/full/10.1002/ggge.20192, 2013b.

Kaiser, B.O., Cacace, M., Scheck-Wenderoth, M., and Lewerenz, B.: Characterization of main heat transport processes in the Northeast German Basin: Constraints from 3-D numerical models, Geochemistry, Geophysics, Geosystems, 12, paper: Q07011, https://doi.org/10.1029/2011GC003535, 2011.

Kato, V.: Geothermal Exploration in Uganda, SDG Short Course I on Exploration and Development of Geothermal, Kenya, Google Scholar, 2016.

Kohfahl, C., Post, V.E.A., Hamann, E., Prommer, H., and Simmons, C.T.: Validity and slopes of the linear equation of state for natural brines in salt lake systems, Journal of Hydrology, 523, 190–195, http://dx.doi.org/10.1016/j.jhydrol.2015.01.054, 2015.

Kolawole, F., and Evenick, J.C.: Global distribution of geothermal gradients in sedimentary basins, Geoscience Frontiers, 14 (6), https://doi.org/10.1016/j.gsf.2023.101685, 2023.

Kovács, J., and Erőss, A.: Statistically optimal grouping using combined cluster and discriminant analysis (CCDA) on a geochemical database of thermal karst waters in Budapest, Applied Geochemistry, 84, 76–86, http://dx.doi.org/10.1016/j.apgeochem.2017.05.009, 2017.

Kreyns, P., Genga, X., and Michael, H.A.: The influence of connected heterogeneity on groundwater flow and salinity distributions in coastal volcanic aquifers, Journal of Hydrology, 586, paper: 124863,. https://doi.org/10.1016/j.jhydrol.2020.124863, 2020.

Kun, É., Szabó, Zs., Tóth, Gy., Székvölgyi, K., Baranyai-Gáspár, E., Falus, Gy., Gál, N.E., Mekker, J., Szűcs, A., Vári, Z., Tihanyiné Szép, E., and Maros, Gy.: Hydrogeological and heat transport modelling of the Buda Thermal Karst (Budapest, Hungary), IAH 2024 World Groundwater Congress, paper: 106358, 2024.

Lapwood, E.R.: Convection of a fuid in a porous medium, Mathematical Proceedings of the Cambridge Philosophical Society, 44 (4), 508–521, https://doi.org/10.1017/S030500410002452X, 1948.

Lenkey, L., Mihályka, J., and Paróczi, P.: Review of geothermal conditions of Hungary, Földtani Közlöny, 151 (1), 65–78, https://doi.org/10.23928/foldt.kozl.2021.151.1.65, 2021.

Licour, L.: The geothermal reservoir of Hainaut: the result of thermal convection in a carbonate and sulfate aquifer. Geologica Belgica, 17 (1), 75–81, https://popups.uliege.be/1374-8505/index.php?id=4401, 2014.

Lipsey, L., Pluymaekersb, M., Goldberg, T., van Oversteeg, K., Ghazaryan, L., Cloetingh, S., and van Wees, J.-D.: Numerical modelling of thermal convection in the Luttelgeest carbonate platform, the Netherlands, Geothermics, 64, 135–151, http://dx.doi.org/10.1016/j.geothermics.2016.05.002, 2016.

Lopez, T., Antoine, R., Kerr, Y., Darrozes, J., Rabinowicz, M., Ramillien, G., Cazenave, A., and Genthon, P.: Subsurface
hydrology of the Lake Chad Basin from convection modelling and observations, Surveys in Geophysics, 37, 471–502,
https://doi.org/10.1007/s10712-016-9363-5, 2016.

Mádlné Szőnyi, J., Erőss, A., Havril, T., Poros, Zs., Győri, O., Tóth, Á., Csoma, A., Ronchi, P., and Mindszenty, A.: Fluids,
flow systems and their mineralogical imprints in the Buda Thermal Karst, Földtani Közlöny, 148 (1), 75–96,
https://doi.org/10.23928/foldt.kozl.2018.148.1.75, 2018.

Mádl-Szőnyi, J., and Tóth, Á.: Basin-scale conceptual groundwater flow model for an unconfined and confined thick carbonate
region, Hydrogeology Journal, 23, 1359–1380, https://doi.org/10.1007/s10040-015-1274-x, 2015.

Mádl-Szőnyi, J., and Tóth, Á.: Topographically driven fluid flow at the boundary of confined and unconfined sub-basins of
carbonates: basic pattern and evaluation approach on the example of Buda thermal Karst, in: Renard, P., Bertrand, C. (Eds.),
EuroKarst 2016, Neuchâtel: Advances in Karst Science. Springer, Cham, 89–98, https://doi.org/10.1007/978-3-319-45465-
8_10, 2017.

Mádl-Szőnyi, J., Batelaan, O., Molson, J., Verweij, H., Jiang, X.-W., Carrillo-Rivera, J.J., and Tóth, Á.: Regional groundwater
flow and the future of hydrogeology: evolving concepts and communication, Hydrogeology Journal, 31, 23–26,
https://doi.org/10.1007/s10040-022-02577-3, 2023.

Mádl-Szőnyi, J., Czauner, B., Iván, V., Tóth, Á., Simon, Sz., Erőss, A., Bodor, P., Havril, T., Boncz, L., and Sőreg, V.:
Confined carbonates – Regional scale hydraulic interaction or isolation?, Marine and Petroleum Geology, 107, 591–612,
https://doi.org/10.1016/j.marpetgeo.2017.06.006, 2019.

Mádl-Szőnyi, J.: Pattern of Groundwater Flow at the Boundary of Unconfined and Confined Carbonate Systems on the
Example of Buda Thermal Karst and its Surroundings (in Hungarian), DSc Thesis, pp. 131, https://real-
d.mtak.hu/id/eprint/1317, 2019.

Magri, F., Inbar, N., Siebert, C., Rosenthal, E., Guttman, J., and Möller, P.: Transient simulations of large-scale
hydrogeological processes causing temperature and salinity anomalies in the Tiberias Basin, Journal of Hydrology, 520,
342–355, https://doi.org/10.1016/j.jhydrol.2014.11.055, 2015.

Magri, F.: Derivation of the coefficients of thermal expansion and compressibility for use in FEFLOW, White Papers III: DHI-
WASY GmbH, Institute for Water Resource Planning and System Research, Berlin, pp. 13–23,
https://hydrosoft.co.kr/sites/default/files/2024-04/Technical_Reference_FEFLOW_white_papers_vol3_ENG.pdf, 2009.

Mersich, I., Práger, T., Ambrózy, P., Hunkár, M., and Dunkel, Z.: Climate Atlas of Hungary (in Hungarian), Hungarian
Meteorological Service, Budapest, p. 107, ISBN: 9637702830, 2003.

Moeck, I.S.: Catalog of geothermal play types based on geologic controls, Renewable and Sustainable Energy Reviews, 37,
867–882, http://dx.doi.org/10.1016/j.rser.2014.05.032, 2014.

Moeck, I.S., and Beardsmore, G.: A new 'geothermal play type' catalog: streamlining exploration decision making,
Proceedings of the Thirty-Ninth Workshop on Geothermal Reservoir Engineering, Stanford University, Stanford,
California, Google Scholar, 2014.

Moeck, I.S., Beardsmore, G., and Harvey, C.C.: Cataloging Worldwide Developed Geothermal Systems by Geothermal Play Type, Proceedings of the World Geothermal Congress, Melbourne, Australia, 19–25, Google Scholar, 2015.

910 Nield, D.A., and Bejan, A.: Convection in Porous Media. (5th ed.), Springer Int, p. 988, https://link.springer.com/book/10.1007/978-3-319-49562-0, 2017.

Nield, D.A.: Onset of thermohaline convection in a porous medium, Water Resources Research, 4 (3), 553–560, https://doi.org/10.1029/WR004i003p00553, 1968.

Noack, V., Scheck-Wenderoth, M., Cacace, M., and Schneider, M.: Influence of fluid flow on the regional thermal field: results

915 from 3D numerical modelling for the area of Brandenburg (North German Basin), Environmental Earth Sciences, 70, 3523–3544, https://doi.org/10.1007/s12665-013-2438-4, 2013.

Ortega Guerrero, M.A.: Numerical analysis of the groundwater flow system and heat transport for sustainable water management in a regional semi-arid basin in Central Mexico, Water, 14, paper: 1377, https://doi.org/10.3390/w14091377, 2022.

920 Otero, J., Dontcheva, L.A., Johnston, H., Worthing, R.A., Kurganov, A., Petrova, G., and Doering, C.R.: High-Rayleigh-number convection in a fluid-saturated porous layer, Journal of Fluid Mechanics, 500, 263–281, https://doi.org/10.1017/S0022112003007298, 2004.

Otieno, V.: Structural controls on fluid pathways in active geothermal systems. Insights from Olkaria Geothermal Field, Kenya, Proceedings World Geothermal Congress, p. 5, Google Scholar, 2020.

925 Özkaymak, Ç., and Sözbilir, H.: Evidence for extensional domain-type geothermal play in western Anatolia: a case study from Afyon-Akşehir Graben, Proceedings World Geothermal Congress, pp. 9, Google Scholar, 2021.

Özler, H.M.: Hydrogeology and geochemistry in the Curuksu (Denizli) hydrothermal field, western Turkey, Environmental Geology, 39 (10), 1169–1180, https://doi.org/10.1007/s002540000139, 2000.

Prol-Ledesma, R.M., and Morán-Zenteno, D.J.: Heat flow and geothermal provinces in Mexico, Geothermics, 78, 183–200,

930 https://doi.org/10.1016/j.geothermics.2018.12.009, 2019.

Pollack, H.N., Hurter, S.J., and Johnson, J.R.: Heat flow from the Earth's interior: Analysis of the global dataset, Reviews of Geophysics, 31 (3), 267–280, https://doi.org/10.1029/93RG01249, 1993.

Pollack, H.N., and Chapman, D.S.: On the regional variation of heat flow, geotherms, and lithospheric thickness, Tectonophysics, 38 (3–4), 1977.

935 Przybycin, A.M., Scheck-Wenderoth, M., and Schneider, M.: The origin of deep geothermal anomalies in the German Molasse Basin: results from 3D numerical models of coupled fluid flow and heat transport, Geothermal Energy, 5 (1), https://doi.org/10.1186/s40517-016-0059-3, 2017.

Robinson, N.I., and Love, A.J.: Hidden channels of groundwater flow in Tóthian drainage basins, Advances in Water Resources 62, 71–78, http://dx.doi.org/10.1016/j.advwatres.2013.10.004, 2013.

940 Rubin, H.: Application of the aquifer's average characteristics for determining the onset of thermohaline convection in a heterogeneous aquifer, Journal of Hydrology, 57 (3–4), 321–336, https://doi.org/10.1016/0022-1694(82)90153-6, 1982a.

Rubin, H.: Thermal convection in a nonhomogeneous aquifer, Journal of Hydrology, 50, 317–331, https://doi.org/10.1016/0022-1694(81)90076-7, 1981.

Rubin, H.: Thermohaline convection in a nonhomogeneous aquifer. Journal of Hydrology, 57 (3–4), 307–320. https://doi.org/10.1016/0022-1694(82)90152-4, 1982b.

Rybach, L.: The geothermal conditions in the Rhine Graben – a summary, Bulletin für Angewandte Geologie, 12 (1), 29–32, Google Scholar, 2007.

Schindler, M., Baumgärtner, J., Gandy, T., Hauffe, P., Hettkamp, T., Menzel, H., Penzkofer, P., Teza, D., Tischner, T., Wahll, G.: Successful hydraulic stimulation techniques for electric power production in the Upper Rhine Graben, Central Europe, Proceedings of the World Geothermal Congress, p. 7, Google Scholar, 2010.

Siler, D.L., and J.E. Faulds, J.E.: Three-dimensional geothermal fairway mapping: Examples from the western Great Basin, USA, Geothermal Resources Council, Google Scholar, 2013.

Simmons, C.T., and Narayan, K.A.: Mixed convection processes below a saline disposal basin, Journal of Hydrology, 194, 263–285, https://doi.org/10.1016/S0022-1694(96)03204-0, 1997.

Simon, Sz., Déri-Takács, J., Szijártó, M., Szél, L., and Mádl-Szőnyi, J.: Wetland management in recharge regions of regional groundwater flow systems with water shortage, Nyírség region, Hungary, Water, 15 (20), paper: 3589, https://doi.org/10.3390/w15203589, 2023.

Smith, L., and Chapman, D.S.: On the thermal effects of groundwater flow: 1. Regional scale systems, Journal of Geophysical Research, 88 (B1), 593–608, https://doi.org/10.1029/JB088iB01p00593, 1983.

Szabó, Zs., Szijártó, M., Tóth, Á., and Mádl-Szőnyi, J.: The significance of groundwater table inclination for nature-based replenishment of groundwater-dependent ecosystems by managed aquifer recharge, Water, 15 (6), paper: 1077, https://doi.org/10.3390/w15061077, 2023.

Szijártó, M., Galsa, A., Tóth, Á., and Mádl-Szőnyi, J.: Numerical investigation of the combined effect of forced and free thermal convection in synthetic groundwater basins, Journal of Hydrology, 572, 364–379, https://doi.org/10.1016/j.jhydrol.2019.03.003, 2019.

Szijártó, M., and Galsa, A.: Thermohaline convection in a homogeneous porous medium, Magyar Geofizika, 61 (4), 177–190, https://epa.oszk.hu/03400/03436/00248/pdf/EPA03436_geofizika_2020_4_177-190.pdf, 2020.

Szijártó, M., Galsa, A., Czauner, B., Erőss, A., Tóth, Á., and Mádl-Szőnyi, J.: Numerical investigation of groundwater ageing and thermal processes in confined unconfined full basins with asymmetric flow pattern, Submitted to Hydrogeology Journal, accepted, 2025.

Szijártó, M., Galsa, A., Tóth, Á., and Mádl-Szőnyi, J.: Numerical analysis of the potential for mixed thermal convection in the Buda Thermal Karst, Hungary, Journal of Hydrology: Regional Studies, 34, paper: 100783, https://doi.org/10.1016/j.ejrh.2021.100783, 2021.

Tóth, Á., Baják, P., Szijártó, M., Tiljander, M., Korkka-Niemi, K., Hendriksson, N., and Mádl-Szőnyi, J.: Multimethodological
revisit of the surface water and groundwater interaction in the Balaton Highland Region — Implications for the overlooked
groundwater component of Lake Balaton, Hungary, Water, 15 (6), paper: 1006, https://doi.org/10.3390/w15061006, 2023.

Tóth, Á., Galsa, A., and Mádl-Szőnyi, J.: Significance of basin asymmetry and regional groundwater flow conditions in
preliminary geothermal potential assessment – Implications on extensional geothermal plays, Global and Planetary Change,
195, paper: 103344, https://doi.org/10.1016/j.gloplacha.2020.103344, 2020.

Tóth, Á., Havril, T., Simon, Sz., Galsa, A., Santos, F.A.M., Müller, I., and Mádl-Szőnyi, J.: Groundwater flow pattern and
related environmental phenomena in complex geologic setting based on integrated model construction: Journal of
Hydrology., 539, 330–344, https://doi.org/10.1016/j.jhydrol.2016.05.038, 2016.

Tóth, J.: A theoretical analysis of groundwater flow in small drainage basin, Journal of Geophysical Research, 68 (16), 4795–
4812, https://doi.org/10.1029/JZ068i016p04795, 1963.

Tóth, J.: A theory of groundwater motion in small drainage basins in central Alberta, Canada, Journal of Geophysical Research,
67 (11), 4375–4387, https://doi.org/10.1029/JZ067i011p04375, 1962.

Tóth, J.: Gravitational systems of groundwater flow: theory, evaluation, utilization, Cambridge University Press, UK, pp. 297,
ISBN: 978–0–521–88638–3, 2009.

Tóth, J.: Groundwater as a geologic agent: An overview of the causes, processes, and manifestations, Hydrogeology Journal,
7, 1–14, https://doi.org/10.1007/s100400050176, 1999.

Tóthi, T., Markó, Á., Szilágyi, I., and Mádl-Szőnyi, J.: Geological risk analysis of geothermal developments in the Buda
thermal karst area, EGU General Assembly 2024, https://doi.org/10.5194/egusphere-egu24-5687, 2024.

Trásy-Havril, T., Szkolnikovics-Simon, Sz., and Mádl-Szőnyi, J.: How complex groundwater flow systems respond to climate
change induced recharge reduction?, Water, 14 (19), paper: 3026, https://doi.org/10.3390/w14193026, 2022.

Tsypin, M., Cacace, M., Guse, B., Güntner, A., and Scheck-Wenderoth, M.: Modeling the influence of climate on groundwater
flow and heat regime in Brandenburg (Germany), Frontiers in Water, 6, paper: 1353394,
https://doi.org/10.3389/frwa.2024.1353394, 2024.

Voss, C.I., Simmons, C.T., and Robinson, N.I.: Three-dimensional benchmark for variable-density flow and transport
simulation: matching semi-analytic stability modes for steady unstable convection in an inclined porous box, Hydrogeology
Journal, 18, 5–23, https://doi.org/10.1007/s10040-009-0556-6, 2010.

Wang, J.-Z., Jiang, X.-W., Wan, L., Wörman, A., Wang, H., Wang, X.-S., and Li, H.: An analytical study on artesian flow
conditions in unconfined-aquifer drainage basins, Water Resources Research, 51 (10), 8658–8667,
https://doi.org/10.1002/2015WR017104, 2015.

Wang, X.S., Jiang, X.-W., Wan, L., Ge, S., and Li, H.: A new analytical solution of topography-driven flow in a drainage basin
with depth-dependent anisotropy of permeability, Water Resources Research, 47, paper: W09603,
https://doi.org/10.1029/2011WR010507, 2011.

Weatherill, D., Simmons, C.T., Voss, C.I., and Robinson, N.I.: Testing density-dependent groundwater models: two-dimensional steady state unstable convection in infinite, finite and inclined porous layers, Advances in Water Resources, 27 (5), 547–562, https://doi.org/10.1016/j.advwatres.2004.01.003, 2004.

1010 Weisbrod, N., Yechieli, Y., Shandalov, S., and Lensky, N.: On the viscosity of natural hyper-saline solutions and its importance: The Dead Sea brines, Journal of Hydrology, 532, 46–51, http://dx.doi.org/10.1016/j.jhydrol.2015.11.036, 2016.

Wendebourg, J., Biteau, J.-J., and Grosjean, Y.: Hydrodynamics and hydrocarbon trapping: Concepts, pitfalls and insights from case studies, Marine and Petroleum Geology, 96, 190–201, https://doi.org/10.1016/j.marpetgeo.2018.05.015, 2018.

1015 Winter, T.C., and Pfannkuch, H.O.: Effect of anisotropy and groundwater system geometry on seepage through lakebeds 2. Numerical simulation analysis, Journal of Hydrology, 75, 239–253, https://doi.org/10.1016/0022-1694(84)90052-0, 1984.

Wooding, R.A.: Steady state free thermal convection of liquid in a saturated permeable medium, Journal of Fluid Mechanics, 2 (3), 273–285, https://doi.org/10.1017/S0022112057000129, 1957.

Yu, C., Shi, H., Miao, Q., Gonçalves, J.M., Dou, X., Hu, Z., Hou, C., Zhao, Y., and Zhang, H.: Impact of irrigation on soil
1020 water balance and salinity at the boundaries of cropland, wasteland and fishponds under a cropland–wasteland–fishpond system, Agronomy, 14 (9), paper: 2110, https://doi.org/10.3390/agronomy14092110, 2024.

Zhang, X., Jiao, J.J., Li, H., Luo, X., and Kuang, X.: Effects of downward intrusion of saline water on nested groundwater flow systems, Water Resources Research, 56, paper: e2020WR028377, https://doi.org/10.1029/2020WR028377, 2020.

Zhang, Z.-Y., Jiang, X.-W., Wang, X.-S., Wan, L., and Wang, J.-Z.: A numerical study on the occurrence of flowing wells in
1025 the discharge area of basins due to the upward hydraulic gradient induced wellbore flow, Hydrological Processes, 32 (11), 1682–1694, https://doi.org/10.1002/hyp.11623, 2018.

Zech, A., Zehner, B., Kolditz, O., and Attinger, S.: Impact of heterogeneous permeability distribution on the groundwater flow systems of a small sedimentary basin, Journal of Hydrology, 532, 90–101, http://dx.doi.org/10.1016/j.jhydrol.2015.11.030, 2016.

1030 Zimmerman, W.B.J.: Multiphysics Modeling with Finite Element Methods, World Scientific Publishing Company, Singapore, p. 432. ISBN: 9812568433, https://doi.org/10.1142/6141, 2006.